The focal adhesion scaffold protein Hic-5 regulates vimentin organization in fibroblasts

Rishel B. Vohnoutka[a,†], Anushree C. Gulvady[a,‡], Gregory Goreczny[a,§], Kyle Alpha[a], Samuel K. Handelman[b], Jonathan Z. Sexton[c], and Christopher E. Turner[a,*]

[a]Department of Cell and Developmental Biology, State University of New York Upstate Medical University, Syracuse, NY 13210; [b]Division of Gastroenterology, Department of Internal Medicine, Michigan Medicine at the University of Michigan, and [c]Department of Medicinal Chemistry, College of Pharmacy, University of Michigan, Ann Arbor, MI 48109

ABSTRACT **Focal adhesion (FA)-stimulated reorganization of the F-actin cytoskeleton regulates cellular size, shape, and mechanical properties. However, FA cross-talk with the intermediate filament cytoskeleton is poorly understood. Genetic ablation of the FA-associated scaffold protein Hic-5 in mouse cancer-associated fibroblasts (CAFs) promoted a dramatic collapse of the vimentin network, which was rescued following EGFP-Hic-5 expression. Vimentin collapse correlated with a loss of detergent-soluble vimentin filament precursors and decreased vimentin S72/S82 phosphorylation. Additionally, fluorescence recovery after photobleaching analysis indicated impaired vimentin dynamics. Microtubule (MT)-associated EB1 tracking and Western blotting of MT posttranslational modifications indicated no change in MT dynamics that could explain the vimentin collapse. However, pharmacological inhibition of the RhoGTPase Cdc42 in Hic-5 knockout CAFs rescued the vimentin collapse, while pan-formin inhibition with SMIFH2 promoted vimentin collapse in Hic-5 heterozygous CAFs. Our results reveal novel regulation of vimentin organization/dynamics by the FA scaffold protein Hic-5 via modulation of RhoGTPases and downstream formin activity.**

Monitoring Editor
Matthew Welch
University of California, Berkeley

Received: Aug 14, 2019
Revised: Oct 10, 2019
Accepted: Oct 18, 2019

INTRODUCTION

Vimentin is a type III intermediate filament (IF; Huber *et al.*, 2015) that is highly expressed in fibroblasts and other mesenchymal cells and is an integral component of the cytoskeleton. Due to the unique structural resiliency of IFs (Eriksson *et al.*, 2009; Huber *et al.*, 2015; Lowery *et al.*, 2015), these proteins play key roles in maintaining the integrity of cells under high mechanical stress, such as during fibroblast-mediated contraction of the extracellular matrix (ECM; Eckes *et al.*, 2000; Wei *et al.*, 2008; Vuoriluoto *et al.*, 2011; Kidd *et al.*, 2014; Costigliola *et al.*, 2017). In addition to their structural function and roles in response to mechanical stimuli, vimentin filaments also regulate cell shape, cell motility, and signal transduction (Eckes *et al.*, 2000; Helfand *et al.*, 2003; Guo *et al.*, 2014; Chernoivanenko *et al.*, 2015). Importantly, modifications in vimentin organization regulate its function in these cellular processes.

Vimentin assembles spontaneously into tetramers that oligomerize into unit-length filaments (ULFs). These assemble further via end-to-end annealing and lateral association to form filaments and filament networks (Engel *et al.*, 1985). In response to extracellular

This article was published online ahead of print in MBoC in Press (http://www.molbiolcell.org/cgi/doi/10.1091/mbc.E19-08-0442) on October 23, 2019.

Author contributions: R.B.V., A.C.G., G.G., and C.E.T. contributed to study conceptualization. R.B.V., A.C.G., and K.A. contributed to experimentation and data curation. Data analysis and statistical assessment were performed by R.B.V., J.Z.S., A.C.G., and S.K.H. R.B.V., K.A., A.C.G., G.G., C.E.T., J.Z.S., and S.K.H. contributed to the writing and editing of the manuscript. Funding acquisition was accomplished by C.E.T.

The authors declare no competing financial interests.

Present addresses: [†]Division of Gastroenterology, Department of Internal Medicine, Michigan Medicine at the University of Michigan, 1150 West Medical Center Drive, Ann Arbor, MI 48109; [‡]Department of Medical Oncology, Dana-Farber Cancer Institute, 450 Brookline Avenue, Boston, MA 02215; [§]Division of Hematology, Department of Medicine, Brigham and Women's Hospital, 75 Francis Street, Boston, MA 02115.

*Address correspondence to: Christopher E. Turner (turnerce@upstate.edu).

Abbreviations used: 3D-CDM, three-dimensional cell-derived matrix; BSA, bovine serum albumin; CAF, cancer-associated fibroblast; ECM, extracellular matrix; FA, focal adhesion; FRAP, fluorescence recovery after photobleaching; Het, heterozygous; HFF, human foreskin fibroblast; IF, intermediate filament; KD, knockdown; KO, knockout; LF, lung fibroblast; MEF, mouse embryonic fibroblast; MFI, mean fluorescence intensity; MT, microtubule; PFA, paraformaldehyde; TIRF, total internal reflectance; ULF, unit-length filament; WT, wild type.

cues, vimentin filaments can reorganize by exchange with filament precursors (tetramers and ULFs) transported by microtubule (MT)- and F-actin–associated motor proteins to support their interactions with other cytoskeletal elements (Leduc and Etienne-Manneville, 2017). Kinase-mediated phosphorylation slows subunit assembly or promotes filament disassembly, while phosphatase-mediated dephosphorylation opposes these effects, together regulating vimentin assembly and reorganization (Eriksson *et al.*, 2004; Snider and Omary, 2014). For example, Rac1 activity within nascent lamellipodia promotes p21-activated kinase (PAK)-mediated vimentin phosphorylation and disassembly (Goto *et al.*, 2002). This localized disassembly of vimentin allows Cdc42 activation of actin nucleation and actin branching enzymes including Arp2/3 and FMNL2/3 formins (Small *et al.*, 2002; Helfand *et al.*, 2011; Kage *et al.*, 2017) and their localization to the cell membrane by Rac1-promoted cortactin recruitment (Weed *et al.*, 2000), ultimately resulting in F-actin–driven force generation and cell membrane protrusion. Vimentin filaments also act as a template for growing MTs during cell polarization (Gan *et al.*, 2016) and regulate organization of integrin-mediated traction forces required for directed cell migration (Costigliola *et al.*, 2017). Therefore, impairment of either Rac1/PAK signaling or vimentin expression impedes directional migration as a result of impaired MT and actin organization in the absence of an intact vimentin cytoskeleton capable of responding to mechanical stimuli (Helfand *et al.*, 2011). Despite increasing evidence of a crucial role for vimentin cross-talk with other cytoskeletal elements in integrating functional cellular responses to mechanical cues, knowledge of the underlying mechanisms for translating these mechanical cues into global vimentin rearrangements that participate in these cellular processes is incomplete.

Recent studies have identified integrin-based cell–ECM adhesions, known as focal adhesions (FAs), as regulators of IF dynamics (Burgstaller *et al.*, 2010; Gregor *et al.*, 2014; Scarpa and Mayor, 2016), although the mechanisms remain unclear. FAs form within lamellipodia of migrating cells, where integrin engagement with the ECM leads to the recruitment of adaptor proteins that link FAs to the F-actin cytoskeleton. The resulting FA–actin associations provide anchoring points on which the cell can exert traction forces for migration (Gardel *et al.*, 2008, 2010; Blangy, 2017; Haage *et al.*, 2018). Actin forms contractile bundles in association with nonmuscle myosin II (called stress fibers) and application of force by these FA-associated stress fibers helps to promote maturation of focal adhesions into fibrillar adhesions (Pankov *et al.*, 2000; Zamir *et al.*, 2000; Goreczny *et al.*, 2018). Conversely, MTs display increased catastrophe rates at FAs (Efimov *et al.*, 2008) and deliver molecules involved in FA disassembly to the FA in a motor protein–dependent manner (Ezratty *et al.*, 2005; Yue *et al.*, 2014). Furthermore, perturbation of MTs with colchicine promotes the maturation of newly formed focal contacts into FAs, suggesting that MTs regulate FA maturation and lifetime negatively (Lloyd *et al.*, 1977; Kaverina *et al.*, 1998). Interestingly, MTs have also been observed to elongate toward immature FAs in the cell periphery, where MT association with the immature FA can result in stabilization of these MTs (Kaverina *et al.*, 1998). Vimentin has been reported to interact directly with FAs via association with the cytoplasmic tails of $\alpha 2\beta 1$ and $\beta 3$ integrins (Kreis *et al.*, 2005; Kim *et al.*, 2016) and indirectly via the linker protein plectin 1f (Bhattacharya *et al.*, 2009; Burgstaller *et al.*, 2010). Vimentin–FA interactions are largely associated with a subset of large, mature FAs (Burgstaller *et al.*, 2010), while vimentin filament precursors (ULFs and tetramers) are present at immature focal complexes, suggesting that vimentin filament coupling to FAs may play a role in FA maturation (Terriac *et al.*, 2017). While the interaction of F-actin and MTs with FAs has been extensively studied, the interactions between vimentin and FAs and the implications of these interactions on the regulation of vimentin organization and function remain poorly understood.

Hic-5 is an important FA adaptor/scaffold protein of the paxillin family (Brown and Turner, 2004; Deakin and Turner, 2008; Deakin *et al.*, 2009, 2012). We have previously shown that ablating Hic-5 in murine cancer-associated fibroblasts (CAFs) promotes F-actin cytoskeleton abnormalities, reduces cell contractility, and decreases the formation of central fibrillar adhesions, thereby reducing extracellular fibronectin remodeling (Goreczny *et al.*, 2017, 2018). Additionally, Hic-5 is up-regulated following TGF-β stimulation (Tumbarello and Turner, 2007) and is associated with the epithelial–mesenchymal transition (Shibanuma *et al.*, 1994; Wang *et al.*, 2008; Pignatelli *et al.*, 2012). It is also important in maintaining an activated fibroblast phenotype (Dabiri *et al.*, 2008) by promoting increased synthesis of ECM components, increased contraction of the ECM, and an increased proportion of mature FAs (Dabiri *et al.*, 2008; Yue *et al.*, 2014; Goreczny *et al.*, 2017).

In the present study, we characterized a collapsed vimentin network and F-actin "hole" phenotype associated with Hic-5 ablation in CAFs, normal lung fibroblasts (LFs), and human foreskin fibroblasts (HFFs). The dynamics of the collapsed vimentin filament network was assessed by fluorescence recovery after photobleaching (FRAP) and Western blot analysis of total and phosphorylated vimentin levels in detergent-insoluble (filamentous) and detergent-soluble (filament precursors) cellular fractions. The phenotype with vimentin collapse and an F-actin hole was recapitulated in Hic-5 heterozygous (Hic-5 Het) CAFs following inhibition of formin activity, while rescue experiments suggest an important role for Hic-5 regulation of Cdc42 activity. These findings provide novel evidence that the FA-associated scaffold protein Hic-5 regulates vimentin dynamics and organization by modulating Rho family GTPases and the activity of formins downstream of these GTPases. Importantly, these data advance our limited knowledge of FA-IF cross-talk.

RESULTS

Hic-5 regulates vimentin organization in cancer-associated and normal fibroblasts

Communication between FAs and IFs has been recently implicated in regulation of FA dynamics and vesicular trafficking to modulate cell migration in normal mesenchymal cells and cells undergoing EMT at sites of tumor formation (Leube *et al.*, 2015; Liu *et al.*, 2015). Coupling of IFs to FAs has been shown previously to increase FA size and strength of adhesion to the matrix while decreasing FA turnover, but the factors that promote IF recruitment to or dissociation from FAs and the subsequent effects on IF organization and dynamics are not known (Tsuruta and Jones, 2003; Bhattacharya *et al.*, 2009; Havel *et al.*, 2015; Osmanagic-Myers *et al.*, 2015). Based on recent studies from our laboratory indicating a role for Hic-5 in promoting FA maturation into fibrillar adhesions in cancer-associated fibroblasts (CAFs; Goreczny *et al.*, 2018), the evidence of a role for IFs in FA and fibrillar adhesion maturation, and previous data that describe a reduction of FA-IF interactions when FA maturation is impaired (Burgstaller *et al.*, 2010), we sought to investigate if Hic-5 has a role in mediating the FA–vimentin intermediate filament cross-talk implicated in these processes.

Hic-5-null CAFs were isolated from a constitutive Hic-5 knockout (KO) murine breast tumor model as previously described: Hic-5 KO mouse, mammary tumor virus-polyomavirus Middle T antigen (MMTV-PyMT) strain (Goreczny *et al.*, 2017, 2018). Hic-5

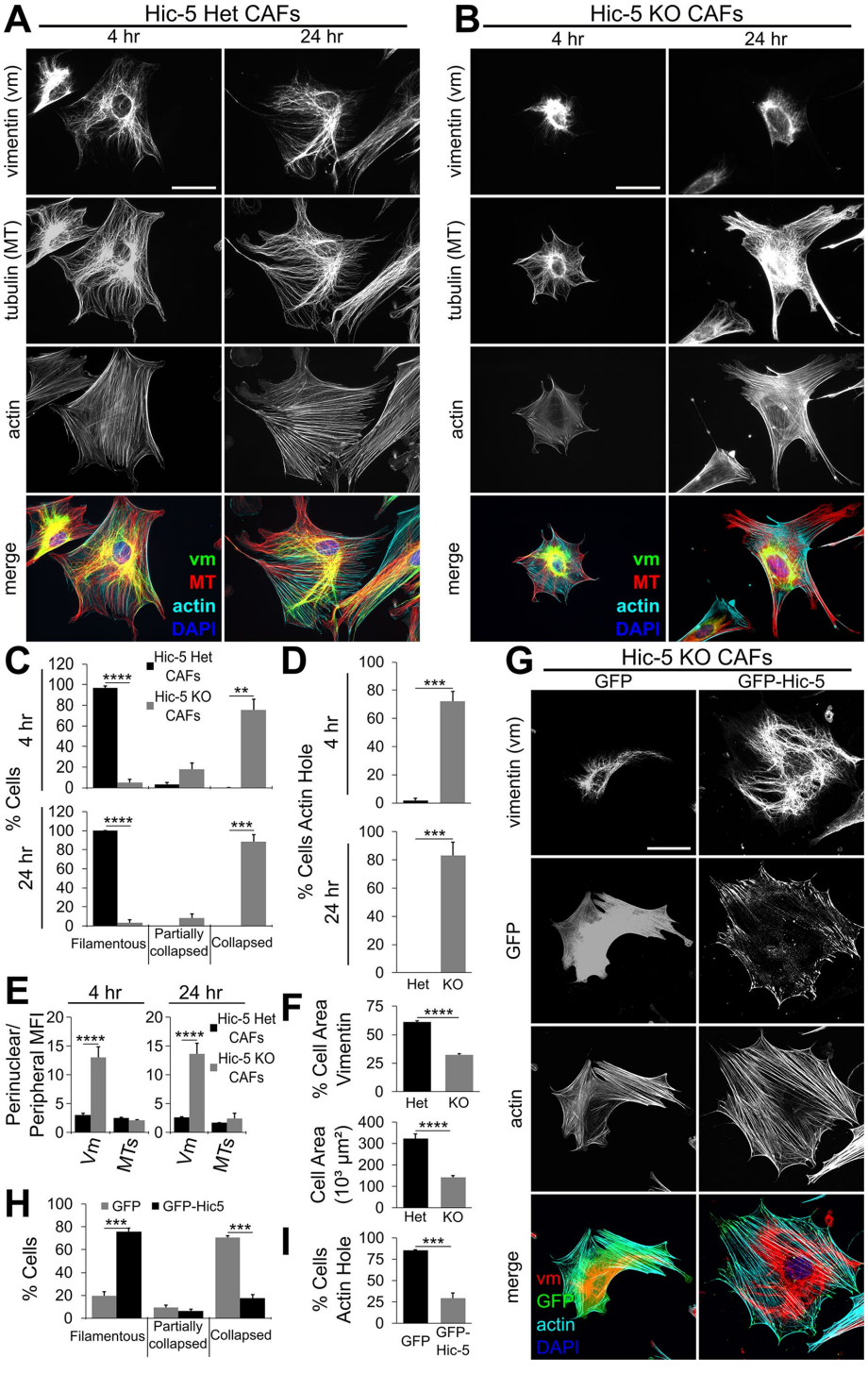

FIGURE 1: Hic-5 regulates vimentin organization in CAFs. (A, B) Representative images of the vimentin, actin, and microtubule cytoskeleton of Hic-5 Het and Hic-5 KO CAFs at 4- and 24-h postplating with (C, D) quantification of the percentage of cells with perinuclear collapse of vimentin and with reduction in centrally located actin stress fibers (actin hole; n = at least 60 cells/condition). (E) Vimentin collapse observed in Hic-5 KO CAFs was also quantified as an increased ratio of perinuclear to peripheral vimentin (n = at least 60 cells/condition). (F) Total cell area and percentage of total cell area occupied by vimentin was decreased in Hic-5 KO CAFs (n = at least 75 cells/condition). (G) Images and (H, I) quantification of exogenous EGFP-Hic-5 rescue of vimentin collapse and the actin hole phenotype 4 h postplating (n = at least 41 cells/condition). All data are shown as the mean ± SEM and are collected from three independent experiments. **, $p < 0.01$; ***, $p < 0.001$; ****, $p < 0.0001$. Scale bar = 50 µm. All CAF experiments were from three unique Hic-5 Het CAF cell lines and one Hic-5 KO CAF cell line.

heterozygote (Het) CAFs were utilized in place of wild-type (WT) CAFs due to the absence of phenotypic differences between WT and Hic-5 Het CAFs and the higher abundance of Hic-5 Het animals available, as previously described (Goreczny *et al.*, 2017). The organization of the three cytoskeletal systems was evaluated by confocal imaging. Visualization of vimentin, the principal IF in fibroblasts, MTs, and F-actin in primary Hic-5 Het and Hic-5 KO CAFs revealed striking differences in F-actin and vimentin cytoskeletal organization (Figure 1, A and B). The vimentin cytoskeleton of Hic-5 KO CAFs was collapsed into closely associated bundles of coaligned vimentin filaments, previously termed "cables" (Hollenbeck *et al.*, 1989), that were restricted to the perinuclear region of the cell, with the collapsed vimentin appearing to coil around the nucleus in some cells. Organization of vimentin was analyzed at an early time point (4 h), when cells are still actively spreading, and a later time point (24 h) post cell plating, corresponding to a fully spread steady state. Vimentin organization was qualitatively classified as filamentous (normal distribution), partially collapsed, or collapsed (see *Materials and Methods* for details). Strikingly, 75–90% of Hic-5 KO CAFs versus 0–3% of Hic-5 Het CAFs were observed to have collapsed vimentin at 4 and 24 h (Figure 1C). Additionally, 72–83% of Hic-5 KO CAFs and 0–10% of Hic-5 Het CAFs were observed to have peripheral F-actin organization with a reduced amount of centrally located F-actin stress fibers ("F-actin hole" phenotype) at 4 and 24 h (Figure 1D), as previously reported (Goreczny *et al.*, 2018). The vimentin collapse and exclusion of actin stress fibers from the area occupied by the collapsed vimentin (the "F-actin hole") is consistent with previous observations of vimentin and actin reorganization following drug-induced MT depolymerization (Hollenbeck *et al.*, 1989). However, MT filament organization (as visualized by α-tubulin staining) was not grossly different between Hic-5 Het and Hic-5 KO CAFs (Figure 1, A and B).

The increase in vimentin staining intensity resulting from compaction and perinuclear localization of vimentin filaments was confirmed with quantitative analyses. Hic-5 KO CAFs displayed a threefold higher ratio of perinuclear/peripheral vimentin mean fluorescence intensity (MFI) than Hic-5 Het CAFs at all time points, while the perinuclear/peripheral ratio of MT MFI was not significantly different between Hic-5 Het and Hic-5 KO CAFs (Figure 1E; see *Materials*

and Methods for details on defining perinuclear and peripheral regions). Additionally, Hic-5 KO CAFs had a 50% reduction in the percentage of cell area occupied by vimentin compared with Hic-5 Het CAFs (Figure 1F), and the total cell area, as measured by F-actin staining, was reduced in Hic-5 KO CAFs (Figure 1F). The vimentin collapse was rescued by exogenous expression of EGFP-Hic-5 in Hic-5 KO CAFs, shifting the percentage of cells with a normal, filamentous distribution of vimentin from 20 to 80% and reducing the percentage of cells with an F-actin hole from 85 to 30% (4-h time point, Figure 1, G–I). Importantly, previous studies have associated vimentin collapse with disruption of the MT cytoskeleton or its associated motor proteins (Hollenbeck *et al.*, 1989; Prahlad *et al.*, 1998; Rathje *et al.*, 2014) and elevated activity of the GTPases Cdc42 and/or Rac1 (Meriane *et al.*, 2000; Chan *et al.*, 2002). Based on the well-documented role of paxillin in regulating Rho family GTPase activity (Turner, 2000; Deakin *et al.*, 2009), MT acetylation (Deakin and Turner, 2014) and paxillin's functional cross-talk, mutual interacting proteins, and extensive structural homology with Hic-5 (Turner, 2000; Brown and Turner, 2004; Deakin and Turner, 2008), we hypothesized that depletion of paxillin may also induce a vimentin phenotype in fibroblasts. However, staining of paxillin KO mouse embryonic fibroblasts (MEFs) showed no indication of either a vimentin collapse or an F-actin hole (Supplemental Figure 1A), indicating that Hic-5 has a nonredundant role in regulating vimentin organization.

Despite their extensive use in the literature (Prahlad *et al.*, 1998; Meriane *et al.*, 2000; Chan *et al.*, 2002; Rathje *et al.*, 2014; Tsui *et al.*, 2018), the methods for vimentin organization analysis described above remain time-inefficient and limited in capability, prompting our use of an automated image analysis pipeline to assess vimentin organization. The Broad Institute Cell Profiler 3.0 software (Carpenter *et al.*, 2006; Jones *et al.*, 2008) was utilized to create a workflow to analyze the distribution of vimentin within the cell via the program's radial distribution module. Consistent with the manual measurements, both the heat map and the graph of vimentin mean fractional intensity, which depicts the distribution of vimentin fluorescence intensity in 16 equal-sized radial bins extending from the center of the nucleus to the outer edge of the cell, show a higher concentration of vimentin localized to a smaller region within the cell (perinuclear localization) in Hic-5 KO CAFs (Figure 2, A–C). Conversely, expression of EGFP-Hic-5 (but not EGFP vector) decreased perinuclear vimentin levels and extended the peak of the vimentin radial distribution further into the peripheral region of the cell (Figure 2, D–F).

Importantly, the CAFs used in these initial studies are fibroblasts converted to an active state within the tumor microenvironment, resulting in inherent modifications to their cytoskeleton that differ from their normal fibroblast counterparts. For example, CAFs often display increased actin stress fibers and elevated α-smooth muscle actin expression (Rasanen and Vaheri, 2010). This causes increased cellular contractility, aiding in CAF-mediated remodeling of the ECM to promote tumor invasion (Rasanen and Vaheri, 2010; Albrengues *et al.*, 2015; Shiga *et al.*, 2015; Kalluri, 2016; Goreczny *et al.*, 2017; LeBleu and Kalluri, 2018). Due to these inherent cytoskeletal differences between CAFs and normal fibroblasts, we also assessed whether Hic-5 depletion induced vimentin collapse in normal lung fibroblasts (LFs) isolated from Hic-5 KO normal (nontumorigenic) mice and in normal human foreskin fibroblasts (HFFs) treated with small interfering RNAs (siRNAs) targeting Hic-5 expression (Figure 3). Hic-5 KO LFs showed a phenotype similar to that of Hic-5 KO CAFs with 68% of cells exhibiting vimentin collapse, as confirmed by a shift toward more perinuclear accumulation of vimentin visualized by automated radial distribution analyses. Additionally, 71% of these cells exhibited an F-actin hole (Figure 3, A–E). Following siRNA-mediated Hic-5 knockdown (KD) in HFFs (Hic-5 KD was 87 ± 5% and 67 ± 5% for Hic-5 siRNA 1 and Hic-5 siRNA 2, respectively; Figure 3, F–H), 61–63% of cells had collapsed vimentin (Figure 3I) associated with a shift in vimentin radial distribution (Figure 3, K and L) and 48–50% had an F-actin hole (Figure 3J). In contrast, RNA interference (RNAi)-mediated depletion of paxillin in HFFs (Deakin and Turner, 2011) failed to induce a vimentin collapse, as was also observed in paxillin KO MEFs (Supplemental Figure 1B). In summary, Hic-5, but not paxillin, is required for establishing and maintaining a filamentous, well-spread vimentin network and the presence of centrally located F-actin stress fibers in normal fibroblasts (LFs and HFFs) and CAFs.

Hic-5 is required for key vimentin phosphorylation events that maintain normal vimentin dynamics, independent of microtubules

We hypothesized that the perinuclear collapse of vimentin filaments observed in Hic-5 KO CAFs represents a shift of cellular vimentin into a hyperassembled state, with potential effects on its phosphorylation status. Importantly, the proportion of filamentous vimentin versus vimentin filament precursors (unit length filaments [ULFs] and tetramers) can be evaluated by fractionating the cell lysate with the detergent Triton X-100. Following centrifugation of the cell lysate, filamentous vimentin pellets (Triton X-100–insoluble material [TX100-insoluble]) and the filament precursors remain in the supernatant (Triton X-100–soluble material [TX100-soluble]; see *Materials and Methods* for details; Shea, 1990; Cheng *et al.*, 2003; Vohnoutka *et al.*, 2017). We therefore analyzed the TX100-insoluble versus TX100-soluble fractions of Hic-5 Het and Hic-5 KO CAFs for total vimentin and vimentin phosphorylated at several key epitopes known to regulate vimentin organization, including phospho-S72, 82, and 55 (Figure 4A; Tsujimura *et al.*, 1994; Goto *et al.*, 1998, 2003; Janosch *et al.*, 2000; Yasui *et al.*, 2001; Cheng *et al.*, 2003; Eriksson *et al.*, 2004; Yamaguchi *et al.*, 2005; Li *et al.*, 2006).

Hic-5 KO CAFs plated for 4 or 24 h had levels of TX100-insoluble vimentin equivalent to that of Hic-5 Het CAFs (Figure 4, A and B). However, Hic-5 KO CAFs had severely reduced TX100-soluble vimentin (Figure 4, A and B). The loss of TX100-soluble vimentin, in the absence of increased TX100-insouble vimentin observed in Hic-5 KO CAFs, indicates either increased proteolysis of TX100-soluble vimentin, as vimentin phosphorylation may modulate IF susceptibility to proteolysis (Zhu *et al.*, 2011), or that the shift of the small population of TX100-soluble vimentin to TX100-insoluble vimentin was below the limit of detectable difference of Western blot analysis. Interestingly, only the TX100-insoluble fractions of Hic-5 Het and Hic-5 KO CAFs were positive for vimentin phospho-epitopes. Hic-5 KO CAFs showed a decrease in both phospho-S72 and phospho-S82 vimentin epitopes in the TX100-insoluble fraction but did not have altered phospho-S55 (Figure 4, C–E). Notably, paxillin KO MEFs did not phenocopy the loss of TX100-soluble vimentin observed in Hic-5 KO CAFs (Supplemental Figure 2A) and paxillin KO MEFs had a significantly higher percentage of total vimentin within the TX100-soluble fraction than Hic-5 KO CAFs (Supplemental Figure 2B). These data indicate that the majority of vimentin within Hic-5 KO CAFs is assembled into vimentin filaments, most likely due to a reduction in the phosphorylation level required to maintain nonassembled, dynamic vimentin.

The decrease in the amount of TX100-soluble vimentin and vimentin phosphorylation in Hic-5 KO CAFs suggests an impairment in vimentin dynamics, which is regulated by these phosphorylation events (Eriksson *et al.*, 2004; Snider and Omary, 2014).

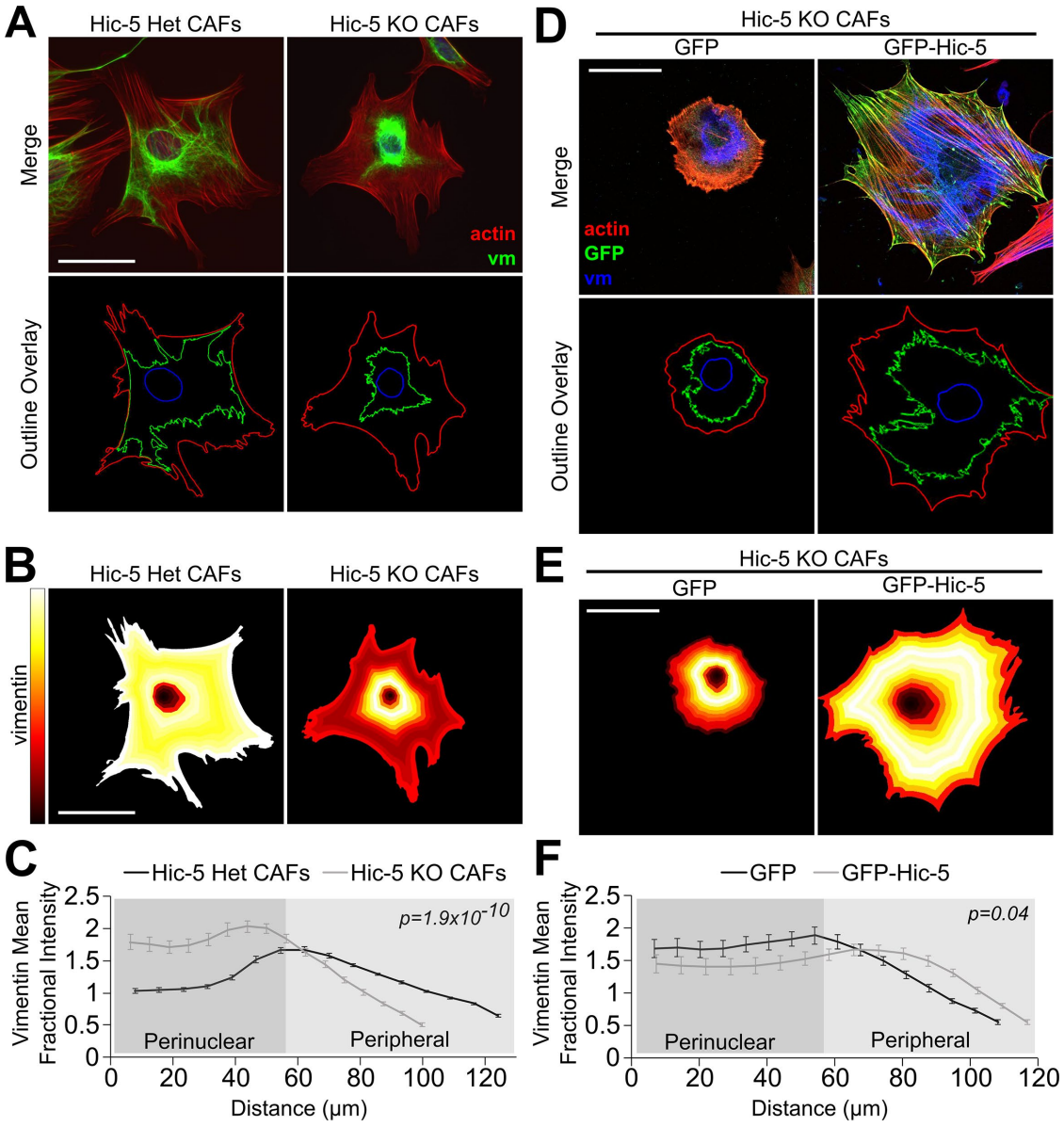

FIGURE 2: Development of a high-throughput image analysis pipeline confirms vimentin collapse in Hic-5 KO CAFs. (A) Merged images of vimentin and actin in Hic-5 Het and Hic-5 KO CAFs at 4 h postplating, alongside the cellular regions identified by the Cell Profiler image analysis pipeline as vimentin or actin. (B) Heat maps of vimentin radial distribution within 16 equal-sized bins from the nucleus to the plasma membrane and (C) quantification of vimentin mean fractional intensity (MFI per bin normalized to number of pixels) across the average major axis length (*x*-axis) of cells in each condition (n = at least 119 cells/condition). (D) Images and (E) heat maps with (F) quantification of vimentin distribution for Hic-5 KO CAFs transfected with EGFP or EGFP-Hic-5 show rescue of the vimentin collapse (n = at least 18 cells/condition). All data are shown as the mean ± SEM and are collected from three independent experiments. Scale bar = 50 μm.

FRAP analyses have been utilized previously to determine the dynamics of IFs in various cell types, with the time for fluorescence recovery in bleached regions of vimentin reported to be 2–8 min for 50% recovery and 11–23 min for full recovery (Yoon *et al.*, 1998; Leduc and Etienne-Manneville, 2017), which is significantly longer than that for actin stress fibers (5–10 min; Hotulainen and Lappalainen, 2006; Campbell and Knight, 2007) or MTs (20 s–6.5 min; Saxton *et al.*, 1984; Omelyanchuk and Munzarova, 2017). To assess possible differences in vimentin dynamics in the presence and absence of Hic-5, we performed FRAP of mCherry-vimentin in Hic-5 Het and Hic-5 KO CAFs (Figure 5; Supplemental Movie S1). The vimentin fluorescence in the bleached zone of Hic-5 Het CAFs recovered to 80% of the prebleach fluorescence intensity in 15 min (900 s), while the vimentin fluorescence of Hic-5 KO CAFs recovered only by 30% in 15 min (Figure 5, A and B). These percentage recoveries indicate that 20 and 70% of the bleached vimentin remained immobile during the bleach recovery period, which corresponds to fluorescence recovery rates of 5 and 2% per minute in Hic-5 Het and Hic-5 KO CAFs, respectively (Figure 5C). Ectopic expression of EGFP-Hic-5 was able to partially rescue the percentage of vimentin fluorescence recovery in Hic-5 KO CAFs to 62%, which corresponds to an immobile fraction of 38% and a

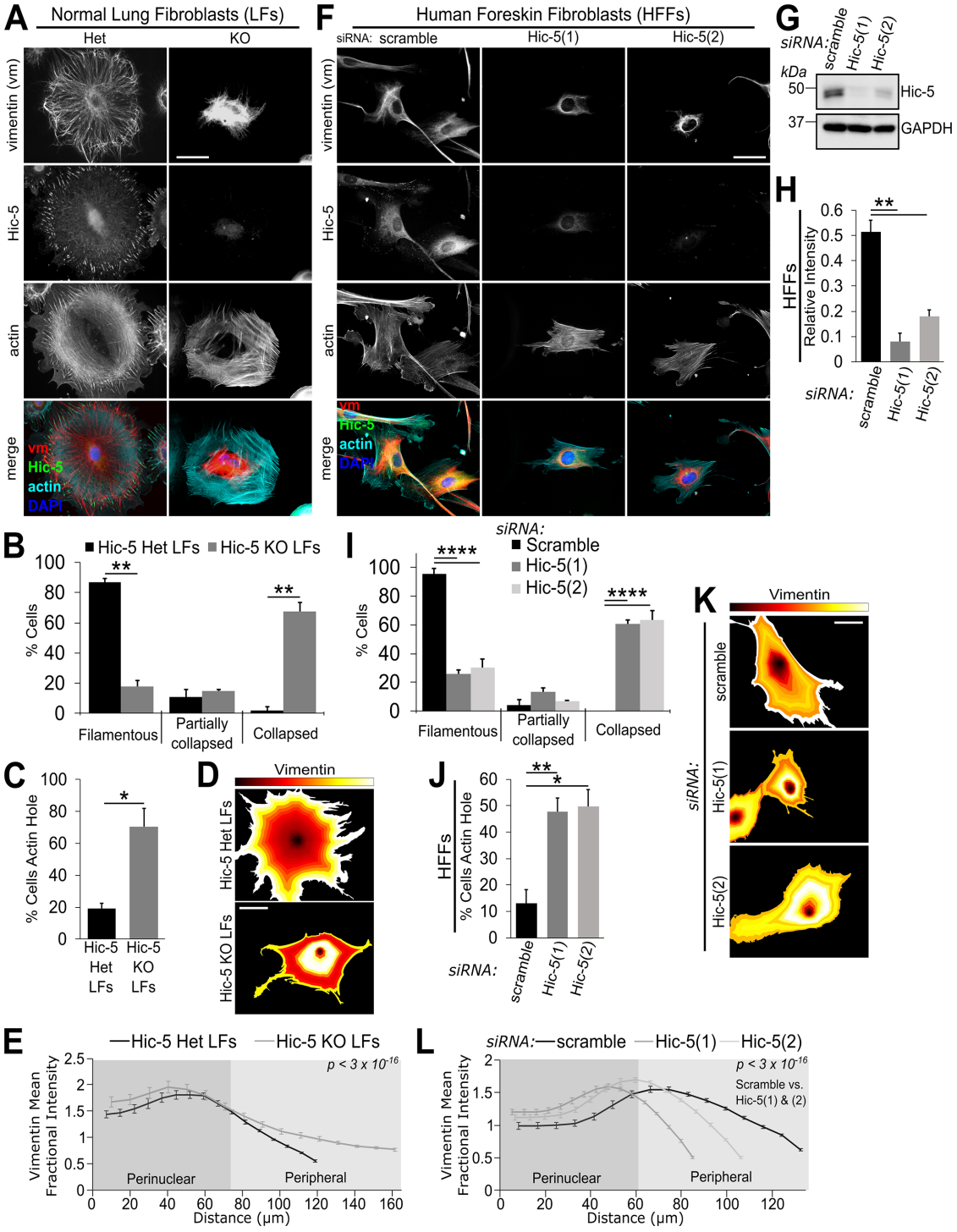

FIGURE 3: Hic-5 regulates vimentin organization in normal mouse and human fibroblasts. (A) Images and (B, C) quantification of percentage of Hic-5 Het and Hic-5 KO normal LFs with collapsed vimentin and an actin hole at 4 h postplating (n = at least 140 cells/condition). (D, E) Vimentin mean fractional intensity showing perinuclear vimentin localization in Hic-5 KO LFs (n = at least 66 cells/condition). (F) Images of HFFs following Hic-5 siRNA KD with (G, H) Western blot analysis of KD efficiency. (I, J) Increased percentage of HFFs with vimentin collapse and an actin hole following Hic-5 depletion (n = at least 102 cells/condition). (K) Corresponding heat maps of HFFs treated with Hic-5 siRNA and (L) graphical representation of this vimentin fluorescence distribution (n = at least 90 cells/condition). All data are shown as the mean ± SEM. Data for LFs (A–E) were collected from two independent experiments, while data from HFFs (F–L) were collected from four independent experiments. * $p < 0.05$; **, $p < 0.01$; ****, $p < 0.0001$. Scale bar = 50 μm. Assessment of HFF cells utilized one HFF cell line obtained from the ATCC, while LF experiments were carried out with two unique Hic-5 Het and two unique Hic-5 KO LF cell lines.

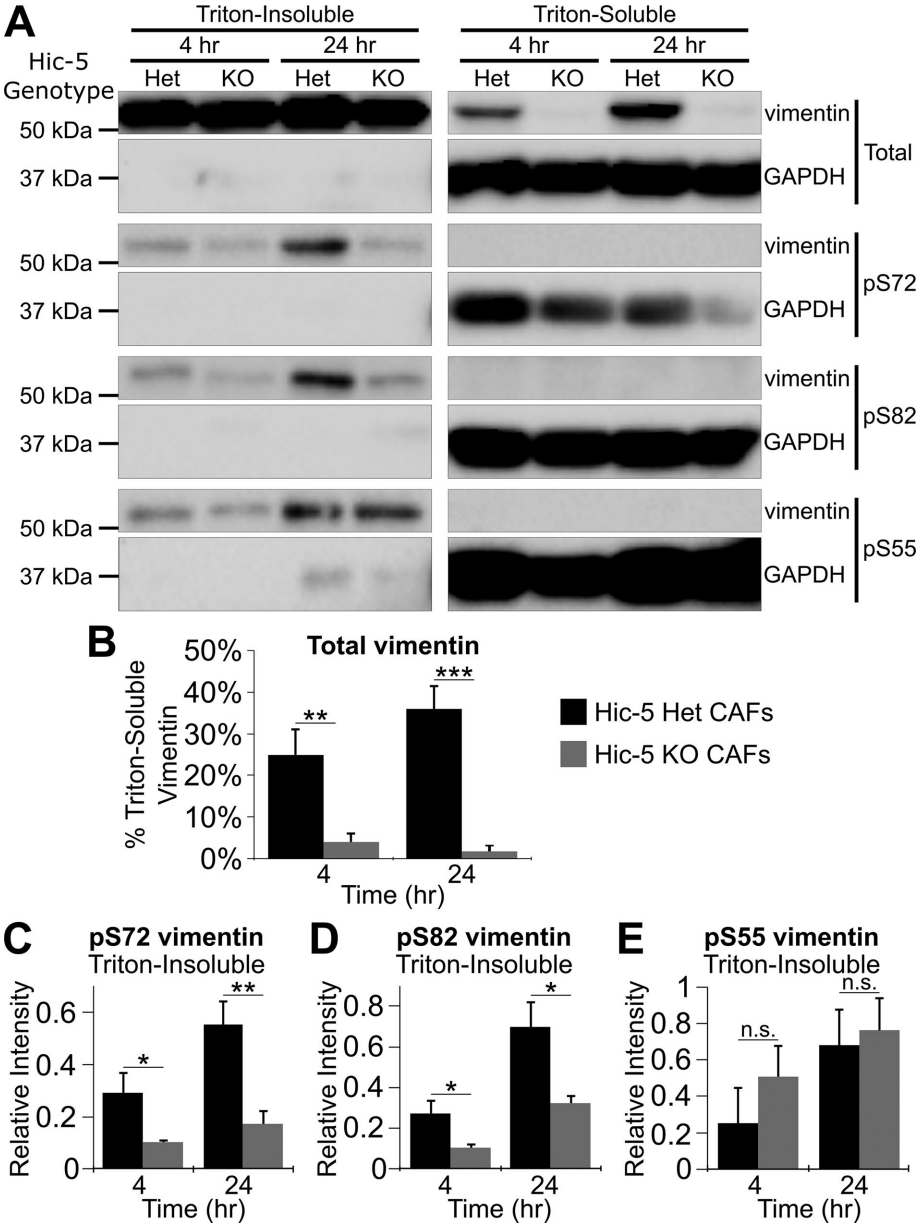

FIGURE 4: Hic-5 ablation reduces vimentin phosphorylation and depletes detergent-soluble vimentin. (A, B) Western blots of Hic-5 Het and Hic-5 KO CAFs at 4 and 24 h reveal a decrease in detergent-soluble vimentin in lysates of Hic-5 KO CAFs. (C–E) Graphs of the level of vimentin phosphorylation analyzed via Western blot with antibodies targeting phospho-S72, -S82, and -S55. All data are shown as the mean relative intensity of the band of interest normalized to the level of soluble GAPDH ± SEM and are collected from at least three independent experiments. * $p < 0.05$; **, $p < 0.01$, *** $p < 0.001$.

recovery rate of 3.6% per minute (Figure 5, D–F; Supplemental Movie S2). These data support the hypothesis that the collapse of the vimentin cytoskeleton in the absence of Hic-5 impairs vimentin phosphorylation and dynamics.

Both IF organization and dynamics have been linked to the integrity of the MT cytoskeleton, as they are dependent on MT-based motor proteins for transport of filament precursors and regulation of vimentin filament distribution by kinesin and dynein (Goldman, 1971; Bershadsky *et al.*, 1991; Prahlad *et al.*, 1998; Rathje *et al.*, 2014; Leduc and Etienne-Manneville, 2017). While our initial assessments revealed no obvious visual alterations in MTs of Hic-5 Het versus Hic-5 KO CAFs (Figure 1), we further investigated whether Hic-5 KO might have promoted vimentin collapse via perturbations of MT posttranslational modifications and/or dynamics. Hic-5 Het and Hic-5 KO CAFs did not show differences in total tubulin, acetylated tubulin, or tyrosinated tubulin by Western blot analyses (Figure 6, A–C). MT dynamics was assessed using the uTrack Matlab plug-in (Jaqaman *et al.*, 2008; Applegate *et al.*, 2011; Ng *et al.*, 2012) to track movement of an EGFP-tagged MT tip protein, EB1-EGFP, in Hic-5 Het and Hic-5 KO CAFs (Figure 6D; Supplemental Movie S3). Importantly, cells expressing the fluorescently tagged MT-labelling peptide, ensconsin microtubule binding domain (EMTD), and EB1 are shown in Figure 6D in order to visualize EB1 localization to MT tips, while cells transfected with EB1 alone were utilized for analyses. These analyses revealed a small but statistically significant increase in the lifetime of MT growth events and the length of MT growth tracks, as well as a decrease in the frequency of MT termination events in Hic-5 KO CAFs compared with Hic-5 Het CAFs (Figure 6, E–G). However, other key measures of MT dynamics, including growth speed of MTs, dynamicity (an overall measurement of MT dynamics where higher values indicate a more dynamic MT cytoskeleton), and number of nucleation events were not altered between Hic-5 Het and Hic-5 KO CAFs (Figure 6, H–J). If Hic-5 depletion caused vimentin collapse via disruption of MTs, we would expect more dynamic MTs with more frequent catastrophe events in the Hic-5 KO cells. Thus, the mechanism of Hic-5 KO–mediated vimentin collapse is independent of MTs. These data collectively indicate that Hic-5 KO induces alterations in vimentin phosphorylation that promote a less dynamic vimentin cytoskeleton lacking the normal subpopulation of dynamic vimentin filament precursors. While this change in vimentin dynamics does not appear to be induced by alterations in MTs, the small increase in MT growth following Hic-5 KO may indicate compensation for the loss of a functional IF cytoskeleton.

Hic-5 regulates vimentin organization and dynamics by modulating RhoGTPases and formin-mediated actin organization

Elevation of Cdc42 and Rac1 RhoGTPase activity has been shown to induce vimentin collapse in cultured fibroblasts (Meriane *et al.*, 2000; Chan *et al.*, 2002), and we have previously shown that Hic-5 KD in human MDA-MB-231 breast epithelial tumor cells alters RhoGTPase signaling (Deakin *et al.*, 2009, 2012; Deakin and Turner, 2011). Importantly, the disruptions in actin organization, including the reduced centrally located actin stress fibers, impaired contraction of collagen gels, and reduction in mature FAs observed in Hic-5 KO CAFs (Figure 1; Engel *et al.*, 1985;

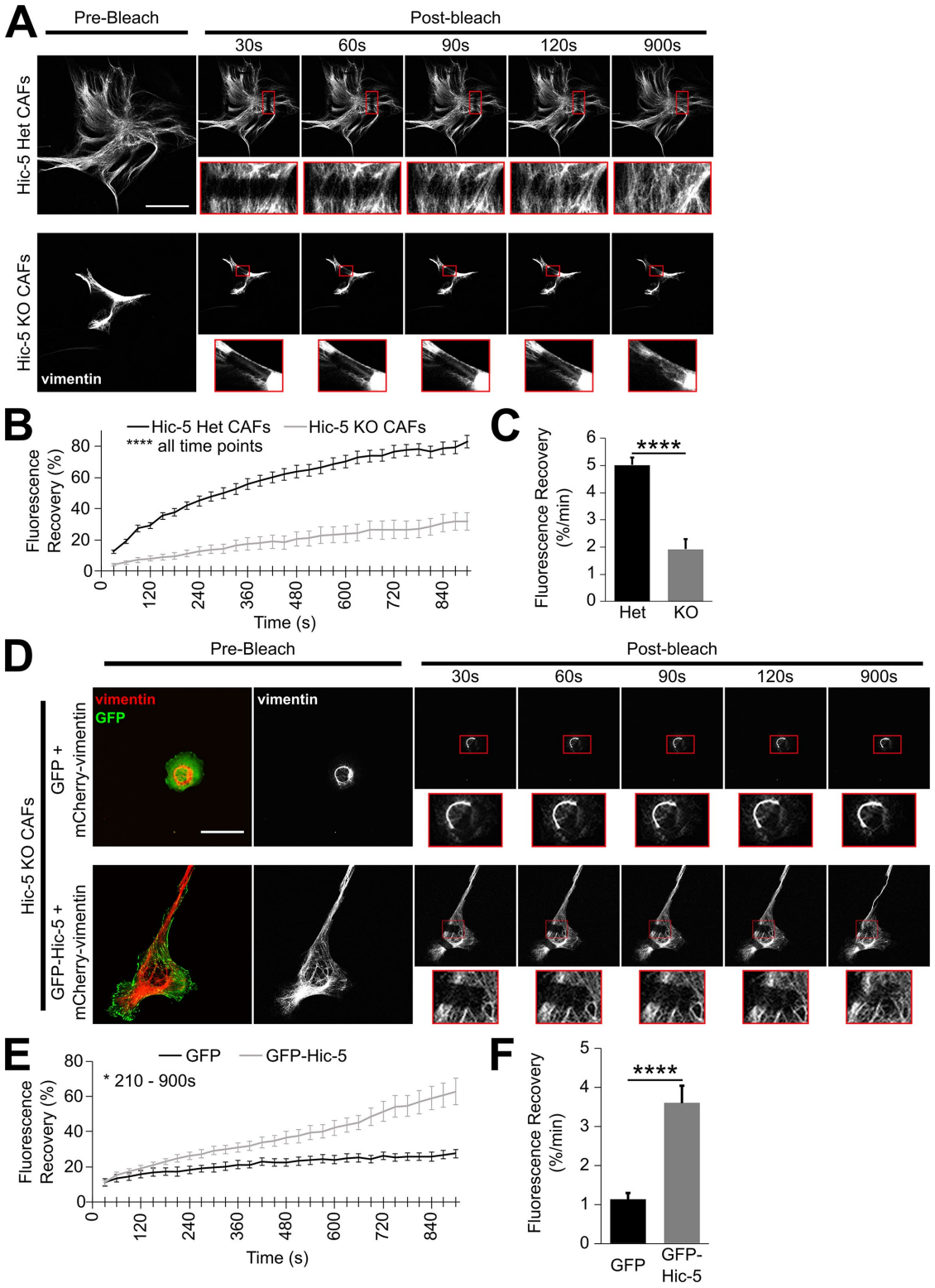

FIGURE 5: Depletion of Hic-5 reduces vimentin dynamics. (A) Individual frames from confocal movies of Hic-5 Het and Hic-5 KO CAFs transfected with mCherry–vimentin subjected to FRAP analysis (Supplemental Movie S1) indicate a marked reduction in vimentin dynamics. Insets depict regions where mCherry–vimentin was bleached and recovery followed over 15 min (1 frame/30 s). (B, C) Quantification of % fluorescence recovery and rate of fluorescence recovery of mCherry–vimentin with measurements of fluorescence values normalized for whole-frame bleaching induced by repeated imaging (n = at least 8 cells/condition). (D) Individual frames of FRAP experiments in which Hic-5 KO CAFs were transfected with mCherry–vimentin and EGFP or EGFP-Hic-5 (Supplemental Movie S2). (E, F) Quantification of the % fluorescence recovery and rate of fluorescence recovery of mCherry–vimentin (n = at least 8 cells/condition). All data represent the mean ± SEM and are collected from three independent experiments. * $p < 0.05$; ****, $p < 0.0001$. Scale bar = 50 μm.

Goreczny *et al.*, 2018), are consistent with impaired activity of the RhoGTPase RhoA and potentially increased activity of the opposing Cdc42/Rac1GTPases (Liu and Burridge, 2000; Spiering and Hodgson, 2011; Matsukawa *et al.*, 2018). To assess the potential role of elevated Cdc42 and/or Rac1 activity in the Hic-5 KO–mediated vimentin collapse, we treated Hic-5 KO CAFs with either a Cdc42 pharmacologic inhibitor (50 μM Zcl278) or a Rac1 inhibitor (100 μM NSC23766; Figure 7A). Inhibition of Cdc42, but not Rac1, was able to rescue the vimentin collapse in Hic-5 KO CAFs from 76% to 20% of cells displaying vimentin collapse (Figure 7B). Interestingly, both Cdc42 and Rac1 inhibition also decreased the percentage of cells with an F-actin hole from 62% to 16 and 41%, respectively (Figure 7C). Inhibition of Cdc42 activity resulted in a significant reduction in peak height and increase in peak width of vimentin radial distribution, indicative of vimentin reorganization (Figure 7, D and E). However, this shift in vimentin radial distribution was not observed in cells treated with Rac1 inhibitor (Figure 7, D and E). Additionally, inhibition of Cdc42 increased the average major axis length (size) of Hic-5 KO cells, as indicated by the increased distance on the *x* axis displaying the vimentin radial distribution graph of Cdc42 inhibition (Figure 7E).

Decreased Cdc42/Rac1 activity has also been associated with increased RhoA activity (Kholmanskikh *et al.*, 2003; Zhang *et al.*, 2007), which in turn promotes the up-regulation of actin stress fiber formation via multiple mechanisms, including activation of formin family members (Oakes *et al.*, 2017). We chose to focus on investigation of formin-mediated actin polymerization because of the known role of formins in the formation/growth of FA-associated actin stress fibers (Burridge and Guilluy, 2016; Livne and Geiger, 2016), coupled with our previous data showing that Hic-5 KO cells exhibit reduced centrally located actin stress fibers resulting from impaired tensin-1–mediated coupling of actin stress fibers with FAs during their maturation to fibrillar adhesions (Goreczny *et al.*, 2017, 2018). Therefore, we hypothesized that Cdc42 inhibition may rescue the central stress fiber assembly and possibly the vimentin collapse observed in Hic-5 KO CAFs by increasing the activity of the opposing RhoA pathway and RhoA-activation of formins that promote FA-associated stress fiber formation (Burridge and Guilluy, 2016; Livne and Geiger, 2016). To assess the role of formins, we investigated the effects of the pan-formin inhibitor SMIFH2 (30 μM) on vimentin organization in Hic-5 Het CAFs. Strikingly, treatment of Hic-5 Het CAFs with SMIFH2 resulted in both vimentin collapse in 94% of cells and the presence of an F-actin hole in 58% of cells (Figure 7, F–H). SMIFH2-induced vimentin collapse produced a substantial shift in vimentin radial distribution, with a significant increase in peak height, decrease in peak width, and decrease in major axis length, indicative of vimentin collapse and decreased cell size (Figure 7, I and J).

These data suggest that ablation of Hic-5 likely results in changes in RhoGTPase activity, including a shift in the balance of Cdc42 versus RhoA activity, which in turn may promote vimentin collapse and F-actin redistribution either directly or indirectly via regulation of formin activity.

RhoGTPase and formin perturbations of Hic-5 knockout cancer-associated fibroblasts increase the velocity of cancer-associated fibroblast migration in two- and three-dimensional matrix environments

Coordinated RhoGTPase-mediated regulation of MT, actin, and vimentin dynamics/organization is crucial to productive cell migration (Eckes *et al.*, 2000; Eriksson *et al.*, 2009; Ridley, 2015). Both paxillin and Hic-5 have been shown to regulate migration by modulating RhoGTPase activity, FA turnover, distribution of key polarity proteins, MT acetylation, and actin stress fiber formation (Deakin *et al.*, 2009, 2012; Deakin and Turner, 2011, 2014; Goreczny *et al.*, 2018). However, whether Hic-5's role in regulating vimentin collapse alters cell migration has not been investigated. Initial observations revealed that Hic-5 KO CAFs were more motile and migrated at a higher velocity on fibronectin in two-dimensional environments (fibronectin-coated tissue culture dishes) than Hic-5 Het CAFs but did not display alterations in directionality (Figure 8, A and B, directionality not shown; Supplemental Movie S4). Ectopic expression of EGFP-Hic-5 in Hic-5 KO CAFs was able to reduce migration velocity in 2D (Figure 8, C and D; Supplemental Movie S5; trending toward significance). Similar Hic-5–dependent migration changes were also observed in CAFs migrating within a three-dimensional cell-derived matrix (3D-CDM) environment (Supplemental Figure 3, A–D; Supplemental Movies S6 and S7). Importantly, Hic-5 KO resulted in the opposite effect on migration from that seen after vimentin KO in normal MEFs, which has been previously shown to result in impaired directionality and decreased motility (Eckes *et al.*, 1998). In contrast, vimentin KD in our Hic-5 Het CAFs did not affect migration velocity but did reduce migration directionality and persistence (Supplemental Movie S8; Figure 8, E and F, directionality and persistence not shown; KD efficiency of 35.5% ± 9.8%, Figure 8G).

We next investigated whether the phenotypes observed upon Cdc42 and formin inhibition of Hic-5 KO CAFs might be contributing to the motility differences observed in the Hic-5 KO cells. Inhibition of Cdc42 with Zcl278 reduced the migration velocity of Hic-5 KO CAFs (Figure 8, H and I; Supplemental Movie S9), and, unexpectedly, treatment of Hic-5 Het CAFs with the pan-formin inhibitor, SMIFH2 also reduced migration velocity (Figure 8, J–K; Supplemental Movie S10). This reduction in velocity likely indicates that pan-formin inhibition disrupts multiple formins required for actin-driven cell propulsion, while the effects of Hic-5 KO on formin activity are more specific and do not impair formin activity involved in actin-driven cell propulsion. These data indicate that Hic-5 KO–mediated vimentin collapse does not phenocopy the effects of vimentin KD on cellular motility, and the increased migration velocity of Hic-5 KO CAFs is due to altered Rho family GTPase activity, but not to formin-mediated actin stress fiber formation defects.

DISCUSSION

Vimentin organization has been shown to regulate a broad array of important cellular functions and biological processes such as polarized lamellipodia formation (Helfand *et al.*, 2011), directional persistence of migrating cells (Gan *et al.*, 2016), and maintenance of cell–cell junctions during collective cell migration in wound healing and development (Li *et al.*, 2013; Menko *et al.*, 2014; Scarpa and Mayor, 2016). Vimentin also associates with points of integrin attachment to the ECM (FAs), where it interacts with the cytoskeletal linker protein plectin 1f (Burgstaller *et al.*, 2010; Castanon *et al.*, 2013), the cytoplasmic tails of several integrins, and potentially other FA-associated proteins or other cytoskeletal elements (Kreis *et al.*, 2005; Bhattacharya *et al.*, 2009; Havel *et al.*, 2015). These vimentin–FA interactions have been correlated with increased FA size, attachment strength to the ECM, and FA maturation (Tsuruta and Jones, 2003; Bhattacharya *et al.*, 2009; Havel *et al.*, 2015; Liu *et al.*, 2015; Osmanagic-Myers *et al.*, 2015). However, the proteins that mediate or promote these FA–vimentin interactions and the effects of these interactions on the vimentin cytoskeleton are poorly understood despite their clear implications for cellular migration, wound healing, metastasis, and many other important biological processes. We report here a novel FA–vimentin signaling axis coordinated by the FA protein Hic-5. Ablation of Hic-5, but not its

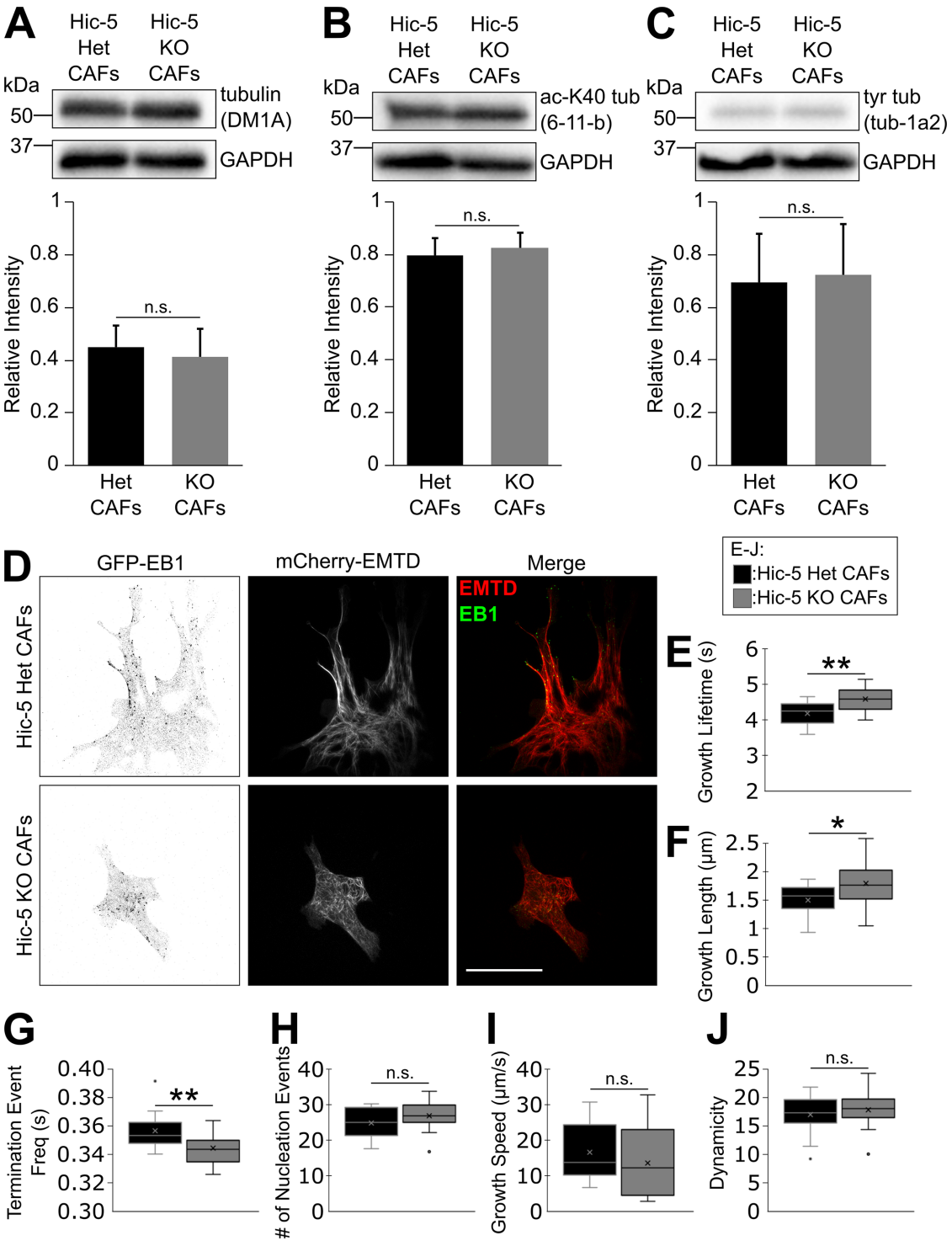

FIGURE 6: Hic-5 regulation of vimentin dynamics is independent of microtubules. (A–C) Western blot of Hic-5 Het and Hic-5 KO CAFs probed with antibodies against α-tubulin (total MT content of cells), acetylated MTs and tyrosinated MTs, accompanied by quantification normalized to GAPDH (data represent the mean ± SEM). (D) Individual frames of Hic-5 Het and Hic-5 KO CAFs transfected with EGFP-EB1 (MT plus end tip protein) and mCherry-EMTD (labels MTs) imaged with TIRF microscopy illustrating EB1 movement and localization to MT tips (Supplemental Movie S3). (E–J) Analysis of MT dynamics of Hic-5 Het and Hic-5 KO CAFs transfected with EB1-EGFP, imaged using TIRF microscopy over 3 min (1 frame/s), and analyzed using a MatLab particle tracker plug-in to track EB1 movement show increased MT growth but no change in overall dynamics in Hic-5 KO CAFs (>157,000 MT tracks/condition). Analyses are plotted as box-and-whisker graphs where the bounds of the box represent the interquartile range, the horizontal line within the box represents the median, and the whiskers represent the range of the data. Data are collected from three independent experiments. *, $p < 0.05$; **, $p < 0.01$. Scale bar = 50 μm.

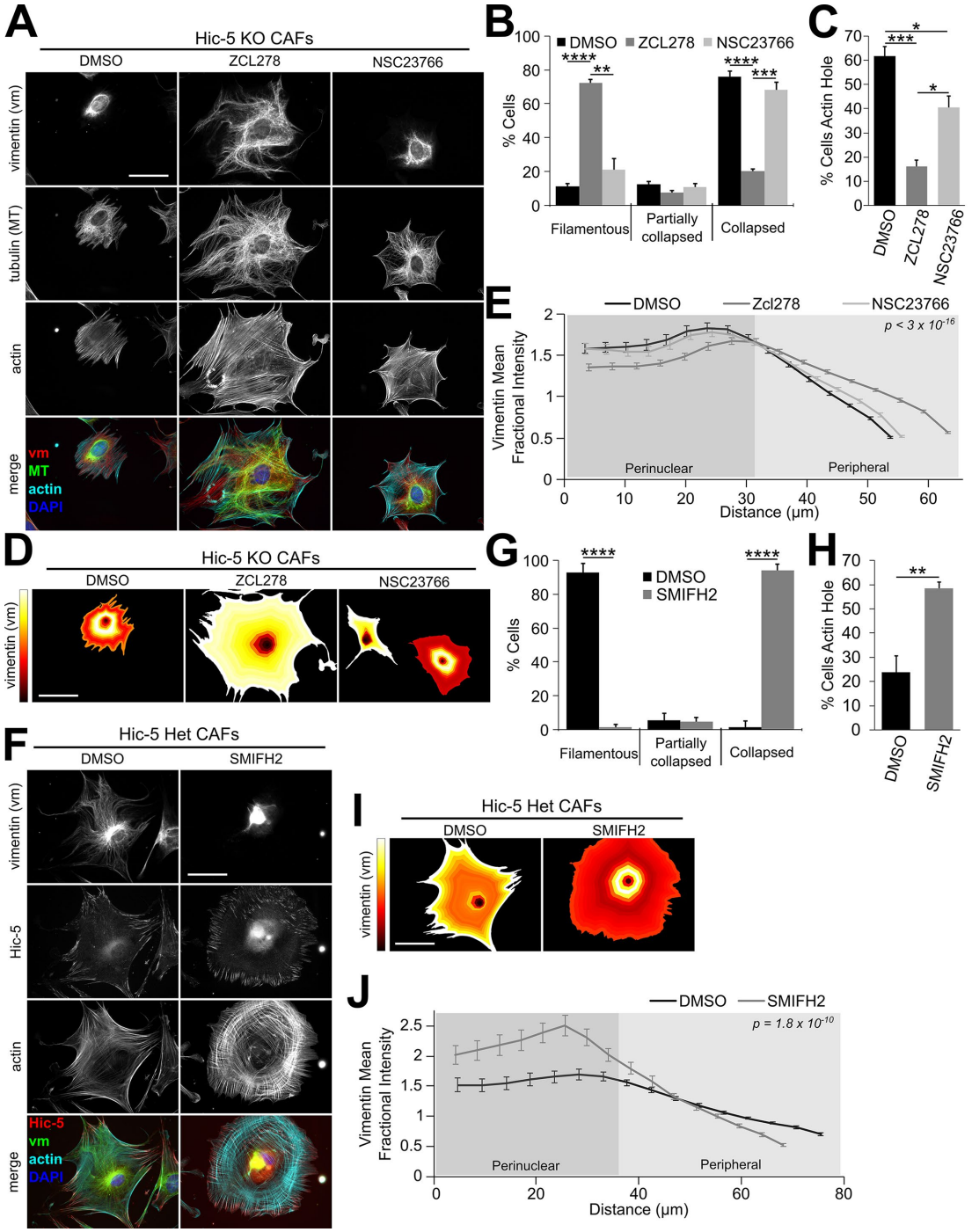

FIGURE 7: Hic-5 regulates vimentin organization via downstream modulation of RhoGTPases and formins. (A) Representative images of Hic-5 KO CAFs treated with a Cdc42 (50 μM Zcl278) or Rac1 (100 μM NSC23766) inhibitor show a reduction in the percentage of cells (B) with vimentin collapse and (C) with an actin hole (n = at least 82 cells/condition cells). (D) Heat maps and (E) quantification of vimentin radial distribution shows a rescue of vimentin organization in Zcl278-treated Hic-5 KO CAFs (n = at least 94 cells/condition). (F) Images and (G, H) quantification of Hic-5 Het CAFs treated with the pan formin inhibitor (30 μM SMIFH2) display reduced percentages of cells with vimentin collapse and an actin hole (n = at least 64 cells/condition). (I) Heat maps and (J) quantification of vimentin radial distribution show induction of vimentin collapse in Hic-5 Het CAFs treated with SMIFH2 (n = at least 70 cells/condition). All data shown represent the mean ± SEM and are collected from three independent experiments. * $p < 0.05$; **, $p < 0.01$; ***, $p < 0.001$, ****, $p < 0.0001$. Scale bar = 50 μm.

close relative paxillin (Brown and Turner, 2004; Deakin and Turner, 2008), was shown to cause a MT-independent collapse of the vimentin cytoskeleton to the perinuclear region of the cell, as well as decreased dynamics and altered phosphorylation status (Figures 1–6; Supplemental Figures 1 and 2). Downstream of Hic-5, we have shown that elevated Cdc42 and, unexpectedly, decreased formin activity were the key causes of the vimentin collapse (Figure 7). These findings represent a previously unobserved pathway

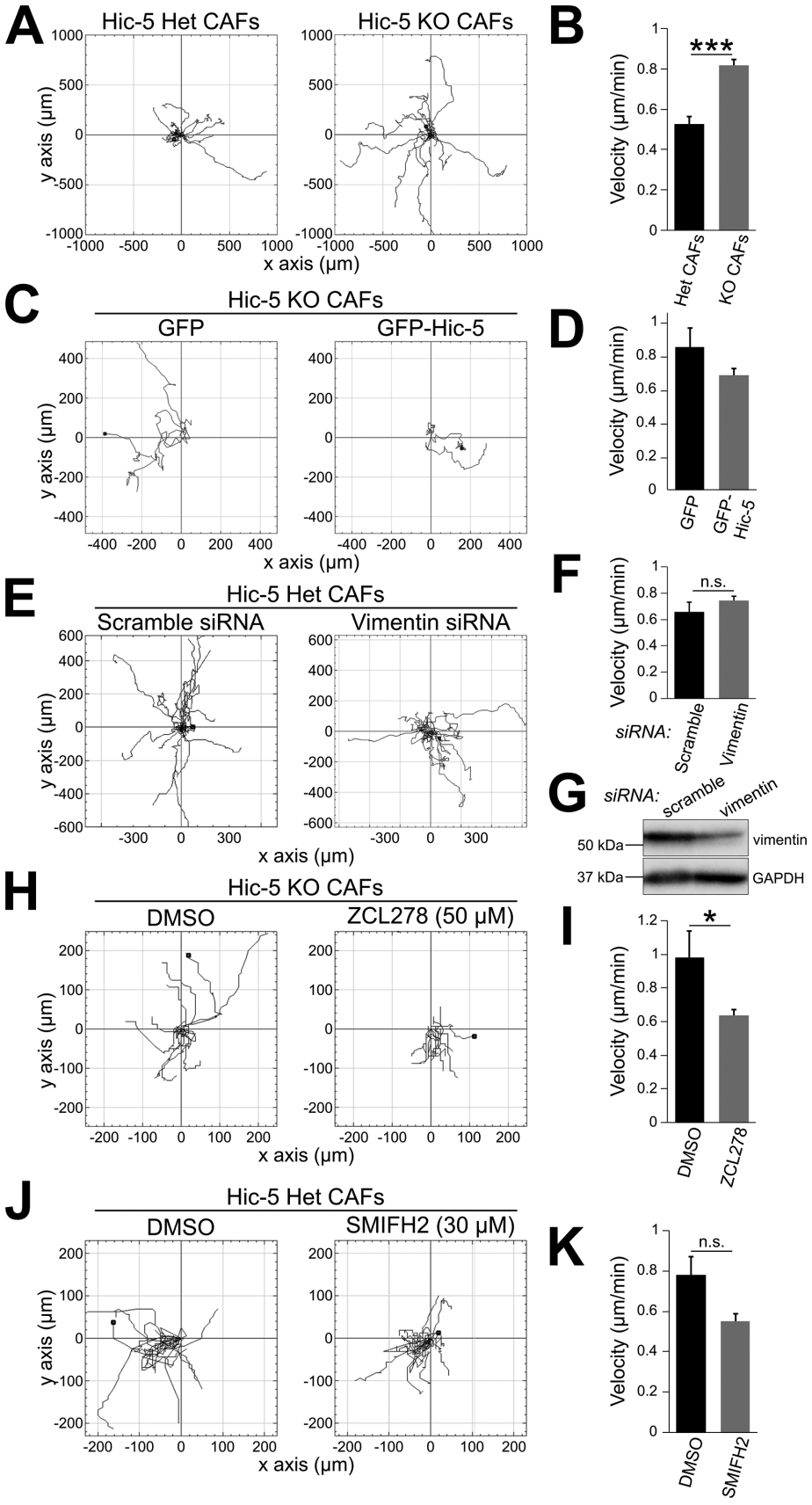

FIGURE 8: Hic-5 modulates migration velocity independent of its effects on vimentin, but through its effects on RhoGTPases. Migration tracks (A, C, E, H, J) of individual cells from cultures of CAFs plated on two-dimensional culture plates coated with fibronectin are shown. Graphs of migration velocity of cells imaged over 16 h (1 image/10 min) are shown for each migration experiment (B, n = at least 60 cells/condition; D, n = at least 28 cells/condition; F, n = at least 47 cells/condition). Cells treated with inhibitors were imaged for 4 h at a frame rate of 1 image/10 min (I, n = at least 55 cells/condition; K, n = at least 85 cells/condition). Western blot was used to assess KD efficiency of vimentin in Hic-5 Het CAFs utilized for migration experiments (G, NT = nontarget siRNA and Vm siRNA = siRNA targeting vimentin transcripts; 35.5% ± 9.8%; $p < 0.05$). All data shown represent the mean ± SEM and are collected from at least three independent experiments. * $p < 0.05$; ***, $p < 0.001$.

through which a FA scaffold protein exhibits cross-talk with the IF cytoskeleton and modulates its organization/dynamics as summarized in Figure 9.

The vimentin reorganization observed in Hic-5 KO CAFs represents a drastic alteration in the dynamics of vimentin and potentially its interaction with other proteins within the cell (Figures 1, 2, 4, and 5). Previous reports indicate that vimentin collapse is a two-step process in which vimentin filaments first undergo exacerbated filament packing to form thick vimentin cables, followed by reorganization of these vimentin cables into a perinuclear mass. Reorganization of the vimentin cables into a collapsed state, but not the formation of cables, is dependent on an intact actin cortex, which was hypothesized to generate the physical force required to mediate vimentin's perinuclear localization (Hollenbeck *et al.*, 1989). The cytoskeletal linker protein plectin1f was later found to be involved in physically linking vimentin to a subset of actin filaments, referred to as transverse arcs, that undergo retrograde flow and therefore exert a perinuclear drag on vimentin filaments (Jiu *et al.*, 2015). Furthermore, siRNA depletion of plectin1f, or specific loss of transverse actin arcs by siRNA depletion of Tm4, in fibroblasts have been shown to promote "overspreading" of the vimentin network to the edge of the cell in circumstances when it would not typically extend this far, such as during cell migration (Jiu *et al.*, 2015). Interestingly, these data suggest that plectin–vimentin interactions at actin arcs, and therefore the maintenance of actin arc formation and actin retrograde flow, are likely retained in the Hic-5 KO CAFs and thus may also contribute to the resulting vimentin collapse. Future analysis of the plectin1f distribution in Hic-5 KO cells is therefore warranted.

In the case of Hic-5 KO–mediated vimentin collapse, these findings are particularly interesting due to the actin abnormalities that were observed in conjunction with

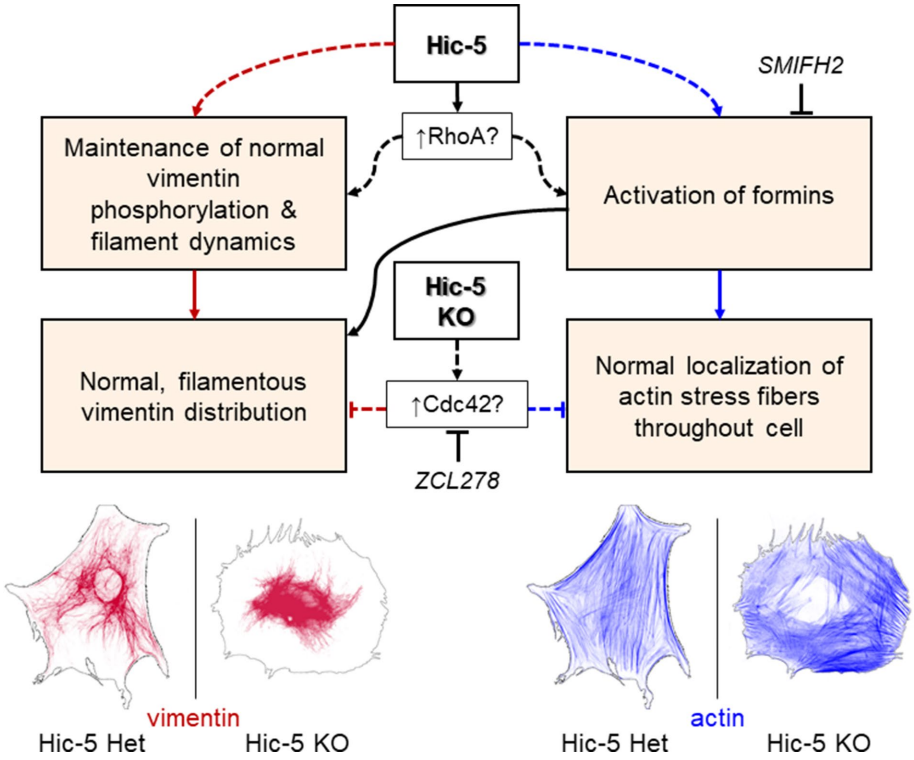

FIGURE 9: Hic-5 regulates vimentin and actin organization via its modulation of RhoGTPases and downstream formin activity. Depletion of the focal adhesion adaptor protein Hic-5 in CAFs and normal fibroblasts results in altered vimentin phosphorylation and vimentin dynamics that are associated with collapse of the vimentin cytoskeleton. Additionally, loss of Hic-5 decreases centrally located actin stress fibers (F-actin hole). These cytoskeleton abnormalities perturb migration dynamics increasing migration velocity of CAFs. Both changes in migration dynamics and abnormalities in vimentin and actin organization are rescued by inhibition of the RhoGTPase Cdc42, while treatment of Het Hic-5 CAFs with the pan formin inhibitor SMIFH2 promotes vimentin collapse and the loss of centrally located actin stress fibers, but not increased migration velocity. These data indicate cross-talk between FAs, vimentin, and actin that may regulate the transition from a promigratory fibroblast (low Hic-5), in which a collapsed vimentin network may allow the cells to navigate through a complex ECM, to a procontractile phenotype (high Hic-5), where increased actin stress fibers and an extended vimentin cytoskeleton promote matrix remodeling.

vimentin collapse (F-actin holes; Goreczny *et al.*, 2017, 2018). If actin retrograde flow of transverse arcs is involved in the Hic-5 KO–mediated vimentin collapse, this suggests that the formation of actin arcs or actin retrograde flow is not ablated in either Hic-5 KO CAFs (Figures 1 and 2) or formin inhibitor–treated CAFs (Figure 7), which is consistent with persistence of peripheral actin structures under both of these conditions. Hic-5 KO may selectively disrupt the formation or maintenance of central FA-associated actin stress fibers, which is consistent with its effects on FA maturation (Goreczny *et al.*, 2018) and the presence of an F-actin hole in Hic-5 KO CAFs. In the case of pharmacological inhibition of formins, this does not inhibit 100% of their activity and the high nucleation efficiency of several formins (Breitsprecher and Goode, 2013), coupled with the specificity of SMIFH2 for formin-mediated actin assembly without affecting activity of other actin nucleation and polymerization enzymes (Rizvi *et al.*, 2009), would result in incomplete actin filament assembly inhibition. This could indicate that Hic-5 KO CAFs have reduced overall actin polymerization, which directly contributes to the F-actin hole, the reduced contractility of cells, the reduction in FA maturation, and the vimentin collapse observed in Hic-5 KO CAFs, without completely ablating actin retrograde flow. This is consistent with the presence of several different kinds of actin stress fibers in fibroblasts (dorsal, ventral, and transverse arcs) that all have different assembly mechanisms and separate regulatory pathways that control their formation and disassembly (Vallenius, 2013). Further perturbation of individual components of actin biology, such as the formation of transverse arcs, utilizing both chemical inhibitors and siRNA KD (such as KD of tropomyosin-4 to disrupt actin arc formation; Jiu *et al.*, 2015), would be of great interest for future studies in order to further investigate this novel connection between formin activity and vimentin organization.

The causes of vimentin collapse observed in other studies are not fully understood, but several different contributing factors have been identified, including chemical perturbation of the MT cytoskeleton that promotes its disassembly (Hollenbeck *et al.*, 1989; Rathje *et al.*, 2014), inhibition of the motor protein kinesin or overexpression/up-regulation of the motor protein dynein (Prahlad *et al.*, 1998), and dysregulation of RhoGTPases and their downstream effectors (Meriane *et al.*, 2000; Chan *et al.*, 2002). In Hic-5 KO CAFs, we have shown that pharmacologic inhibition of Rac1 slightly reduces the percentage of cells with an F-actin hole, while inhibition of Cdc42 efficiently rescues both the vimentin collapse and the F-actin hole phenotype (Figure 7), suggesting that Hic-5 KO promotes vimentin collapse and the loss of central stress fibers via the elevation of Cdc42 activity. It is important to note that the Cdc42 inhibitor utilized for these experiments (Zcl278) has been reported to act through inhibition of the interaction of Cdc42 with one of its activators, the guanine nucleotide exchange factor intersectin-1 (Friesland *et al.*, 2013). Interestingly, exogenous expression of intersectin-1 in human lung cancer cells has been associated with vimentin collapse (Jeganathan *et al.*, 2016). However, the regulation of RhoGTPases and their effects on cytoskeleton and cell shape may have opposing effects in epithelial cells and in fibroblasts (Deakin *et al.*, 2012). Furthermore, Zcl278 binds directly to the site on Cdc42 where intersectin-1 binds, which affects the ability of intersectin-1 to activate Cdc42, but does not affect other functions of intersectin-1 that may otherwise induce vimentin collapse (Friesland *et al.*, 2013). These findings could suggest that Hic-5 may have a direct role in intersectin-1–mediated activation of Cdc42. However, our data more strongly support a mechanism in which Hic-5 KO leads to reduced RhoA activity, in turn promoting increased Cdc42 and Rac1 activity and a corresponding decrease in the activity of certain formins, leading to vimentin collapse (Figure 9).

As discussed, the actin abnormalities and subsequent rescue of both actin and vimentin abnormalities following Cdc42 inhibition in Hic-5 KO CAFs are consistent with impaired signaling of the opposing RhoA pathway. In particular, GTP-bound RhoA is known to bind to several formins crucial for FA-associated stress fiber formation and contribute to their conversion from an autoinhibited state to an

active state. This suggests that Hic-5 KO may reduce the activity of several formins via a reduction in RhoA activity and a corresponding elevation in Cdc42/Rac1 activity (Lammers *et al.*, 2005; Rose *et al.*, 2005; Kuhn and Geyer, 2014). Furthermore, vimentin collapse associated with increased Cdc42/Rac1 signaling was previously shown to be mediated by the activation of two of their downstream targets, PAK and p70 S6 kinase, which phosphorylate vimentin at S72, S55, and multiple other sites (Chan *et al.*, 2002). In Hic-5 KO CAFs, we observed changes in the level of phosphorylation of several key vimentin phosphorylation sites known to regulate its assembly, including a decrease in S72 and S82 phosphorylation, but no difference in phosphorylation of S55 (Figure 4). This shift in vimentin phosphorylation likely contributes to both the loss of soluble vimentin (Figure 4) and the reduction in vimentin dynamics (Figure 5).

Interestingly, the vimentin phosphorylation epitopes were detected in the TX100-insoluble fraction of vimentin, but not the TX100-soluble fraction, in both Hic-5 Het and Hic-5 KO CAFs. We hypothesize that this is in part due to the common use of phosphatase inhibitors before cell lysis, fractionation, and the assessment of vimentin phosphorylation in studies that observe soluble phosphorylated vimentin. These phosphatase inhibitors artificially stabilize vimentin phosphorylation and elevate the levels of TX100-soluble vimentin (Eriksson *et al.*, 2004). It has previously been hypothesized that in cells not treated with phosphatase inhibitors, phosphatases would likely display a preference for soluble vimentin subunits in order to maintain the low levels of TX100-soluble vimentin normally observed in the absence of phosphatase inhibitors/pharmacological enrichment of vimentin phosphorylation (Eriksson *et al.*, 2004). Therefore, in the absence of phosphatase inhibitors, phosphatase preference for soluble vimentin subunits would result in low levels of soluble vimentin phosphorylation and would promote reincorporation of soluble subunits into vimentin filaments over accumulation of the soluble subunits. In addition, other studies have neglected to investigate vimentin phosphorylation in CAFs, which are likely to have more TX100-insoluble vimentin than normal fibroblasts due to their activated, contractile status, associated with their growth within the tumor ECM, which displays a much higher rigidity than normal ECM (Murray *et al.*, 2014). It will be of interest to further probe which specific kinases are acting downstream of Hic-5 to regulate vimentin organization and to perform a comprehensive phosphoproteomic analysis of Hic-5–dependent regulation of vimentin phosphorylation. Subsequent use of kinase inhibitors and/or site-directed mutagenesis of key vimentin phosphorylation consensus sites may be successful in addressing their respective roles in Hic-5–dependent organization of the vimentin network. However, to the best of our knowledge, there is no single phospho site mutation of vimentin known to cause network collapse, while mutation of one or more phospho sites in keratin IFs has been shown to promote their collapse, suggesting a complex interrelationship (Kakade *et al.*, 2016; Sawant *et al.*, 2018).

The dysregulation of Rho GTPases in Hic-5 KO CAFs may also stimulate the changes in fibroblast migration observed on two- and three-dimensional substrates (Figure 8; Supplemental Figure 3). RhoA promotes the formation of actin stress fibers, which, along with actin retrograde flow, have been shown to promote migration in mesenchymal cells (Anderson *et al.*, 2008; Vallenius, 2013; Katsuno *et al.*, 2015; Inagaki and Katsuno, 2017). However, Hic-5 KO CAFs migrate faster (Figure 8, A and B) than their Hic-5 Het counterparts despite having reduced actin stress fibers (Figure 1) as well as impaired RhoA signaling, likely due to elevation of Cdc42 (Figure 7). Increased migration velocity in cells with small numbers of actin stress fibers has been noted in several additional cell types including immune cells (macrophages and leukocytes; Friedl and Wolf, 2003, 2010). Surprisingly, depletion of RhoA/B in macrophages also increased their migration velocity and phosphomyosin light chain level, a component of actin stress fibers that mediates their contractility (Friedl and Wolf, 2010). These seemingly conflicting observations are the result of different modes of cell migration (mainly amoeboid versus mesenchymal) that employ unique profiles of actin dynamics and FA composition, lifetime, and interaction with the ECM to facilitate cell migration (Abercrombie *et al.*, 1970a–c; Lauffenburger and Horwitz, 1996; Friedl and Wolf, 2003, 2010; Ridley *et al.*, 2003; Madsen and Sahai, 2010; Sixt, 2012). Cancer cells can switch between amoeboid and mesenchymal modes of migration (referred to as plasticity), and this has been shown to be reciprocally regulated by Hic-5 and paxillin (Deakin and Turner, 2011; Gulvady *et al.*, 2018). While fibroblasts have not been observed to exhibit a similar amoeboid mode of migration, the regulation of cancer cell plasticity by Hic-5 does support a role for this protein in modulating the type of migration a cell employs. This is likely mediated through Hic-5 RhoGTPase-dependent modulation of actin dynamics and possibly through RhoGTPase cross-talk with the vimentin cytoskeleton, as observed in a recent study connecting RhoGTPase modulation of vimentin organization to integrin α6β4 signaling and cellular migration dynamics in transformed epithelial cells (Colburn and Jones, 2018).

In normal fibroblasts, RhoA-stimulated stress fiber formation is precisely balanced with Cdc42/Rac1 activation of PAK and other kinases, which promotes efficient turnover of FAs (Rane and Minden, 2014). In Hic-5 KO CAFs, we have shown that FA turnover is accelerated (Goreczny *et al.*, 2018) and that inhibition of Cdc42 rescues cytoskeletal abnormalities observed in Hic-5 KO CAFs. Additionally, vimentin association with FAs has been shown to increase FA size and lifetime (Burgstaller *et al.*, 2010), which suggests that Hic-5 localization to the FA may regulate FA lifetime both through its previously shown effects on FA association with actin stress fibers and through a novel function of recruiting vimentin to FAs via modulation of RhoGTPase activity. Thus, our results support a role for Hic-5 in regulating the velocity of fibroblast migration via modulating RhoGTPase activity and recruitment of vimentin to the cell periphery, where vimentin may interact with FAs to promote their maturation.

Here, we have identified key signaling events regulated by Hic-5 that mediate dramatic changes in vimentin organization. Nevertheless, it is also likely that physical interactions involving Hic-5 at FAs play a role in vimentin organization and F-actin–vimentin crosstalk. For example, Hic-5 could spatially promote activation of Cdc42 via its recruitment of guanine nucleotide exchange factors (GEFs) and GTPase activating proteins (GAPs), including its binding partners βPIX/GIT/VAV2 (Yu *et al.*, 2010). Indeed, vimentin has also been shown to interact with VAV2 (Havel *et al.*, 2015). Alternatively, Hic-5 could serve as a physical linker of vimentin to FAs, possibly via either direct interactions with tensin (Goreczny *et al.*, 2018) or potentially plectin1f, both of which are known to associate with fibrillar adhesions, a mature subset of FAs involved in fibronectin fibrillogenesis and thereby ECM remodeling (Burgstaller *et al.*, 2010; Goreczny *et al.*, 2018). However, any such additional physical interactions appear not to be essential, as pharmacologic Cdc42 inhibition rescues vimentin collapse in the absence of Hic-5 (Figures 7 and 9). Although less likely, Hic-5 could also play a role in regulating the activity or location of these signaling proteins, by binding or sequestering them in the cytosol. Last, due to vimentin collapse following acute treatment with siRNA

targeting Hic-5 expression, it is unlikely that Hic-5 regulates vimentin organization via its well-documented roles in regulation of global changes in gene expression (Heitzer and DeFranco, 2006). Future studies investigating which of the many domains of Hic-5 (Brown and Turner, 2004; Gulvady *et al.*, 2018) are required for regulating vimentin organization would be of value in further elucidating the molecular pathways involved.

In conclusion, the data described herein identify a novel role for Hic-5 as a regulator of vimentin organization and dynamics via its modulation of RhoGTPase and formin activity. Hic-5 also regulates the switch from a migrating fibroblast (low Hic-5 expression) to a more contractile fibroblast with reduced migration and increased contraction and matrix remodeling of the ECM (high Hic-5 expression). Collapsed vimentin, associated with low levels of Hic-5 expression (KD and KO), may represent a unique cytoskeletal organization that allows a promigratory phenotype of fibroblasts through a dense ECM network where vimentin expression has been shown to impair migration velocity (Patteson *et al.*, 2018). Similarly, the relationship between RhoGTPase-mediated regulation of formins and vimentin collapse represents a signaling axis that may also contribute significantly to the transition of fibroblasts from a migratory state to a contractile state at the site of wound healing or within the tumor stroma.

MATERIALS AND METHODS

Cell lines, reagents, chemicals, and antibodies

CAFs were isolated from tumors of Hic-5 Het (+/-) and Hic-5 KO (-/-) PyMT mice as previously described (Goreczny *et al.*, 2017). Hic-5 Het and Hic-5 KO normal lung fibroblasts (LFs) were isolated from Hic-5 Het and Hic-5 KO mice using a slightly modified version of the protocol used to isolate CAFs (Goreczny *et al.*, 2017) where the lungs were isolated as previously described (Seluanov *et al.*, 2010). Human foreskin fibroblasts (HFFs) were obtained from the American Type Culture Collection (ATCC), and paxillin knockout (-/-) mouse embryonic fibroblasts (KO MEFs) (Hagel *et al.*, 2002) were a generous gift from S. Thomas (Harvard Medical School, Cambridge, MA).

CAFs and normal LFs were cultured in a 1:1 mixture of DMEM:Ham's F12, while all other cell lines were cultured in 100% DMEM. All media were supplemented with 10% fetal bovine serum (Atlanta Biologicals; vol/vol), 2 mM L-glutamate, 10 I.U./ml penicillin, 10 µg/ml streptomycin, and 1 mM sodium pyruvate. Cells were maintained in a 37°C humidified incubator with 5% CO_2. All cell lines utilized were routinely checked for mycoplasma contamination via 4′,6-diamidino-2-phenylindole (DAPI) staining.

The following antibodies were used in this study for Western blot (WB) and IF analyses: mouse anti-vimentin (Abcam: VI-10; IF—1:500), chicken anti-vimentin (Abcam: ab24525; IF—1:500), rabbit anti-vimentin (Cell Signaling Technologies: D21H3; WB—1:1000), rabbit anti-phospho-S72 vimentin (Abcam: EP1070Y; WB—1:5000), rabbit anti-phospho-S82 vimentin (Abcam: EP1071Y; WB—1:5000), mouse anti-phospho-S55 vimentin (Abcam: 4A4; WB—1:400), mouse anti-α tubulin (Sigma: Dm1a; WB—1:2000; IF—1:200), mouse anti-acetyl-α tubulin (EMD Millipore: 6-11B-1, recognizes acetylated K40; WB—1:1000), mouse anti-tyrosinated-α tubulin (Invitrogen: TUB-1A2; WB—1:1000), mouse anti-GAPDH (Proteintech: 1E6D9; WB—1:2000), mouse anti-Hic-5 (BD Biosciences: Clone 34; WB—1:1000; IF—1:100), and mouse anti-GFP (Santa Cruz Biotechnology: sc-9996, 1:200). For visualization of F-actin and the nucleus, cells were stained with Acti-stain 555- or Acti-stain 670-conjugated phalloidin (Cytoskeleton: PHDH1 or PHDN1; 1:1000), and DAPI (Sigma-Aldrich; 10 µg/ml), respectively. Anti-mouse immunoglobulin G (IgG), anti-rabbit IgG, or anti-chicken IgG conjugated to Alexa Fluor 488, 550, or 633 (Thermo Fisher Scientific) were used as secondary antibodies for all immunofluorescence experiments.

The following pharmacological inhibitors were also utilized: the Cdc42 inhibitor Zcl278 (Cayman Chemicals; 50 µM), the Rac1 inhibitor NSC23766 (EMD Millipore; 100 µM) and the pan-formin inhibitor SMIFH2 (Calbiochem; 30 µM).

RNAi and transfections

Hic-5 and vimentin protein expression was depleted in HFFs and CAFs, respectively, via transfection with siRNA. Cells were plated onto plastic tissue culture dishes, allowed to adhere for 24 h, and then transfected with 10 µM siRNA using RNAiMAX (Life Technologies) transfection reagent per the manufacturer's instructions. After 24 h, transfection complexes were removed by media change and cells were incubated for an additional 24 h in growth media to allow adequate depletion of transcripts and proteins. Following KD, cells were replated on fibronectin for subsequent analysis. KD efficiency was routinely assessed by immunoblotting and was found to be 87 ± 5% and 67 ± 5% for Hic-5 siRNA 1 and 2, respectively, and 35.5% ± 9.8% for vimentin siRNA. RNAi-mediated depletion of Paxillin (KD) in HFFs was assessed by immunofluorescence staining for paxillin and cytoskeletal arrangement was analyzed in cells with paxillin staining (control) versus without paxillin staining (KD).

Oligomers used in this study included nontargeting control siRNA ("NT siRNA"; Dharmacon), a pool of four siRNA targeting mouse vimentin transcripts ("Vm siRNA"; Dharmacon SMARTpool ON-TARGETplus siRNA L-061596-01), one of two siRNA targeting human Hic-5 transcripts (Hic-5 siRNA 1 and Hic-5 siRNA 2; Deakin and Turner, 2011; Pignatelli *et al.*, 2012; Gulvady *et al.*, 2018) or siRNA targeting human paxillin transcripts (Deakin and Turner, 2011). Hic-5 siRNA oligonucleotides were purchased from Life Technologies (catalogue number AM16106) and their sequences were as follows: Hic-5–1, 5′-GGAGCUGGAUAGACUGAUG-3′; Hic-5–2, 5′-GGACCAGUCUGAAGAUAAG-3′. Paxillin siRNA oligonucleotides were purchased from Ambion with the following sequence: paxillin-2, 5′-GUGUGGAGCCUUCUUUGGU-3′.

For overexpression experiments, cultures were transfected using Lipofectamine 3000 (Thermo Fisher Scientific) according to the manufacturer's instructions, except for the DNA amount. Cells were grown for 24 h following plating of 50,000 cells per condition and then transfected for 24 h with the appropriate construct. For vimentin collapse and migration rescue experiments, Hic-5 KO CAFs were transfected with 5 µg EGFP or EGFP-Hic-5 (Gulvady *et al.*, 2018). For rescue of vimentin FRAP, Hic-5 KO CAFs were transfected with 4 µg mCherry-vimentin (a generous gift from Michael Davidson [Addgene plasmid # 55158; http://n2t.net/addgene:55158; RRID:Addgene_55158]) and 4 µg of either EGFP vector or EGFP-Hic-5. For assessment of microtubule dynamics, Hic-5 Het or Hic-5 KO CAFs were transfected with either 3 µg EB1-EGFP (JB131; Addgene plasmid number: 39299; gift from Tim Mitchison and Jennifer Tirnauer, Harvard Medical School) or with both 3 µg EB1-EGFP and 3 µg ensconsin microtubule binding domain–2x mCherry (EMTD-mCherry; Addgene plasmid number: 26742; Miller and Bement, 2009). Finally, cells were replated and allowed to adhere for 4 h on the appropriate substrate for subsequent downstream analyses (see below for more details).

Immunofluorescence microscopy and analysis

Cells were plated onto fibronectin-coated glass coverslips (12 × 1.5 mm) for 4 h before fixation unless otherwise stated (cells were spread for 2 or 24 h where indicated). All fibronectin-coated surfaces for cell plating were prepared by incubation with 10 µg/ml

fibronectin diluted in phosphate-buffered saline (PBS) containing magnesium and calcium for 24 h at 4°C. Following cell adherence, cells were washed once in prewarmed PHEM buffer (pH 7.2; 120 mM PIPES, 50 mM HEPES, 20 mM ethylene glycol-bis(β-aminoethyl ether)-*N*,*N*,*N*′,*N*′-tetraacetic acid [EGTA], 4 mM magnesium sulfate) and then fixed with 4% (wt/vol) paraformaldehyde (PFA) in PBS (pH 7.2) at 37°C for 15 min. Following fixation, free aldehyde groups were quenched for 15 min with 100 mM glycine in PBS. Cells were then permeabilized and blocked by incubation in 3% bovine serum albumin (BSA) diluted in PBS containing 0.25% (vol/vol) Triton X-100 and incubated overnight at 4°C with primary antibodies diluted in blocking buffer. Next, cells were washed three times with PBS + 0.1% Tween-20 (vol/vol) and stained for 1 h with the appropriate secondary antibodies (as well as DAPI and phalloidin where indicated) diluted in blocking buffer. Finally, cells were washed three times with PBS + 0.1% Tween-20 and mounted on glass slides with Gelvatol (10% [wt/vol] polyvinyl alcohol, 20% [vol/vol] glycerol, 0.5 M Tris-HCl, pH 8.5). Cells were imaged using a Leica SP8 laser scanning confocal microscope with a Plan Apochromat 63×/1.4 NA oil λ BL objective or a Zeiss Axioskop2 plus microscope fitted with a Q-Imaging ExiBlue charge-coupled device camera using an Apochromat 40×/0.75 NA oil objective. For analyses of vimentin collapse and the presence of an F-actin hole, described below, a minimum of three independent experiments with at least 20 cells per experiment were quantified (except for normal LFs, of which a minimum of 66 cells were analyzed from two independent experiments).

Cells were analyzed for vimentin collapse and for the presence of an F-actin hole. Vimentin collapse was visually defined by two identifying characteristics: 1) collapsed vimentin had higher-intensity staining than filamentous vimentin due to bundling into closely associated vimentin filaments called thick vimentin cables (Hollenbeck *et al.*, 1989) and 2) the collapsed vimentin occupied a smaller area within the cell than filamentous vimentin. By observing these characteristics, cells were qualitatively assessed as having one of three vimentin phenotypes: filamentous (normal distribution), partially collapsed, or collapsed vimentin. Cells with a filamentous distribution of vimentin exhibited a normal perinuclear cage of vimentin surrounding the nucleus and an array of filaments extending toward the periphery of the cell. In cells with collapsed vimentin, the network of peripheral vimentin filaments is lost and replaced by the formation of thick vimentin cables localized to the perinuclear region of the cell. Cells with partially collapsed vimentin also displayed a perinuclear localization of vimentin, but with some normal vimentin filaments remaining extended toward the cell periphery. Additionally, cells were visually assessed and classified as having a normal F-actin distribution or as having a reduced number of centrally located actin stress fibers compared with their corresponding controls (Goreczny *et al.*, 2017). These analyses were expressed as percentages of cells with an F-actin hole.

Qualitative differences in vimentin distribution were also confirmed with the following quantitative measurements using FIJI software: a ratio of perinuclear vimentin mean fluorescence intensity (MFI) to peripheral vimentin MFI and the percentage of total cell area occupied by vimentin. For regional fluorescence measurements, F-actin staining with phalloidin was used to define the total area of the cell (actin mask). Four points located at 50% of the distance from the edge of the nucleus to the outer edge of the actin mask were marked, and each point was connected to define the perinuclear region of the cell. In cells in which regions of the nucleus contacted the outer edge of the cell, the perinuclear mask was drawn to the edge of the nucleus at points of nucleus–cell membrane contact. The peripheral region of the cell was then defined as the area of a cell extending from the edge of the actin mask to the edge of the perinuclear region of the cell. The areas occupied by actin (total cell area) and vimentin were measured using the threshold function in FIJI and these values were expressed as the % total cell area occupied by vimentin: (area occupied by vimentin ÷ area occupied by actin) × 100.

Additionally, a high-throughput automated analysis pipeline for measuring vimentin collapse was designed in Cell Profiler 3.0 to facilitate quantification of large image sets and to provide a publicly available tool for future analyses of vimentin organization. The manual analyses of vimentin collapse described above and utilized in Figure 1 was utilized to train and validate the analysis pipeline. The software was configured to identify a mask of the area occupied by the actin signal and a mask of the area occupied by the vimentin signal on a per-cell basis. The area occupied by the nucleus was removed from both masks. Adjustments in the range of fluorescence values used to define a positive signal (presence of actin or vimentin) were made on a per-experiment basis. The accuracy of mask identification was manually confirmed for each cell using the outline overlay output of the Cell Profiler pipeline. Outliers in which the analysis pipeline was not able to accurately identify the actin and vimentin masks were removed from the data analysis output. Additionally, for analysis of vimentin radial distribution in cells transfected with EGFP vector or EGFP-Hic-5, a minimum threshold of total EGFP fluorescence was set to select for EGFP-expressing cells only.

Fluorescence values for vimentin were then collected from within the vimentin mask and the radial distribution function of Cell Profiler was used to display their distribution across the total cell area (actin mask). The vimentin distribution was calculated across 16 bins defined by dividing the area from the center of the nucleus to the edge of the actin mask into 16 segments of equal area. Vimentin mean fractional intensity was used to measure the amount of vimentin within each bin. This measurement is calculated as the average fluorescence intensity per pixel at a given distance from the nucleus, normalized to the total intensity of the cell. As fluorescence is generally proportionate to target abundance, this normalized per-pixel measure corresponds to the relative protein concentration as a function of distance from the nucleus. Results were displayed as a heatmap of vimentin distribution from the Cell Profiler output and as a line graph of the average of each bin's mean fractional vimentin intensity versus the bin distance from the nucleus. Bin sizes represent the distance of the outer edge of each bin from the center of the nucleus (μm) and were calculated on a per-condition basis for each experiment using the major axis length parameter calculated by Cell Profiler and the following formula: (major axis length ÷ 16) × (bin number).

Inhibitor treatments

For inhibitor treatments, cells were incubated at 37°C for 2 h post-plating before treatment with Zcl278, NSC23766, or SMIFH2 for 4 h as indicated. Cells treated with inhibitors for migration experiments were imaged during the 4-h treatment, while cells treated with inhibitors for immunofluorescence experiments were fixed following the 4-h inhibitor treatment. All inhibitor treatments were compared with a vehicle control, dimethyl sulfoxide (DMSO), for assessment of their cellular effects.

Triton fractionation of cell lysates

The amount of assembled filamentous vimentin versus vimentin filament precursors was assessed by fractionation of Hic-5 Het and Hic-5 KO CAF lysates with the detergent Triton X-100 (TX100). Cells were grown on fibronectin-coated plastic tissue culture dishes for 4

or 24 h before cellular protein was harvested by lysis in 1X cell lysis buffer (50 mM Tris-HCl, pH 7.2, 5 mM EGTA, 120 mM sodium chloride, 10 mM magnesium chloride, 1% TX100, 1X protease inhibitor cocktail from Roche Diagnostics, 1X PhosStop from Roche Diagnostics, and 1 mM phenylmethylsulfonyl fluoride [PMSF]). Cell lysates were centrifuged at 10,000 × *g* for 10 min at 4°C and the supernatant was transferred to a new tube (Triton-soluble vimentin filament precursors) and the pellet (Triton-insoluble filamentous vimentin) was resuspended in 1X cell lysis buffer with 8M urea and 1% SDS. The TX100-soluble fraction of each sample was normalized according to total protein content as determined by a Pierce bicinchoninic acid protein assay kit (Thermo Fisher Scientific) and TX100-insoluble fractions were normalized based on the soluble fractions' protein concentration. All fractions were diluted using 4X Laemmli buffer with 2.5% (vol/vol) β-mercaptoethanol. Samples were boiled for 5 min and then run on SDS–PAGE gels with 15 µg total protein or 25% of the total lysate volume (for samples lysed directly into sample buffer, such as samples used for confirmation of knockdown) loaded per lane. Proteins were then transferred for 1 h to nitrocellulose membranes. Nitrocellulose membranes were blocked with 3% BSA in Tris-buffered saline with 0.1% Tween-20 (TBST) and incubated with primary antibodies diluted in 1.5% BSA in TBST overnight at 4°C. Next, nitrocellulose membranes were washed three times with TBST and incubated with the horseradish peroxidase (HRP)-conjugated secondary antibodies (anti-mouse IgG or anti-rabbit IgG) diluted 1:10,000 in 1.5% BSA-TBST for 1 h at room temperature. After three TBST washes, immunoblots were visualized with enhanced chemiluminescence substrate (SuperSignal West; Thermo Fisher Scientific) and imaged using a ChemiDoc MP (BioRad). Relative band intensities were measured using FIJI software and normalized to each sample's corresponding GAPDH loading control. TX100-insoluble fractions were normalized to the GAPDH loading control of their corresponding TX100-soluble fraction.

Fluorescence recovery after photobleaching

Hic-5 Het and Hic-5 KO CAFs transfected with mCherry–vimentin with EGFP or mCherry–vimentin with EGFP/EGFP-Hic-5 and plated onto fibronectin-coated glass bottom tissue culture dishes (MatTek, No. 1.5) were utilized for vimentin fluorescence recovery after photobleaching (FRAP) and vimentin FRAP rescue experiments, respectively. A Leica SP8 laser scanning confocal microscope equipped with a humidified chamber maintained at 37°C with 5% CO_2 was used for all FRAP analyses with images collected using a Plan Apochromat 63×/1.4 NA oil λ BL objective. During imaging, cells were maintained in live-cell imaging medium (50% phenol red-free DMEM/50% Ham's F12 with supplements described above). Prebleach images were obtained using low-intensity laser power (5%). Regions of similar size were selected from the vimentin channel of each cell and photobleached using 100% laser power for six iterations (~10 s). Recovery of vimentin fluorescence was then monitored at 5% laser power for 15 min with images acquired at 30-s intervals. Vimentin intensity was measured in the photobleached region before and after photobleaching. Intensity values were background-subtracted and normalized to compensate for whole-frame photobleaching caused by repeated imaging using a nonphotobleached region of vimentin within the same cell. All fluorescence intensity values were measured using FIJI software. The percentage and rate of fluorescence recovery in each bleached region at all time points postphotobleaching were then calculated based on the corrected fluorescence values. A minimum of three cells were analyzed from each of three separate experiments with fluorescence recoveries calculated from a total of eight to 22 individual bleached regions.

Total internal reflection fluorescence live-cell imaging of EB1-EGFP and analysis of microtubule dynamics

Hic-5 Het and Hic-5 KO CAFs transfected with EB1-EGFP or EB1-EGFP and EMTB-mCherry and plated onto glass bottom tissue culture dishes (MatTek, No. 1.5) were utilized for live-cell total internal reflection fluorescence (TIRF) microscopy. Cells transfected with both EB1-EGFP and EMTB-mCherry were used to confirm localization of EB1 to the tips of MTs, while cells transfected with only EB1-EGFP were used for analysis of MT dynamics using the u-track 2.2 plug-in for Matlab created by the Danuser Lab at UT Southwestern Medical Center (Jaqaman *et al.*, 2008; Applegate *et al.*, 2011; Ng *et al.*, 2012). Cells were imaged 4 h postplating using a Plan Apochromat 100×/1.4 NA objective and a Nikon Eclipse TE2000-E multimode TIRF microscope equipped with an environmental chamber maintained at 37°C. During imaging, cells were maintained in live-cell imaging medium as described above. Each cell was imaged for 3–5 min at 1-s intervals for single-channel imaging and 5.5-s intervals for two-channel imaging using 488- and 550 nm-lasers. MT dynamic parameters showing a statistical difference between Hic-5 Het and KO CAFs (growth lifetime, growth length, and frequency of termination), as well as three additional key measurements of MT dynamics that did not show a statistical difference (number of nucleation events, growth speed, and dynamicity) were selected from the software output to represent MT dynamics under these two conditions. Five cells each from three separate experiments (15 cells per condition) were quantified for a minimum of 150,000 EB1 tracks per condition.

Three-dimensional cell-derived matrix generation and migration analysis in two and three dimensions

Migration of Hic-5 Het and Hic-5 KO CAFs was assessed on both two-dimensional tissue culture dishes and three-dimensional cell-derived matrices (CDMs). 3D-CDMs were generated using HFFs as described previously (Deakin and Turner, 2011). For live-cell imaging and migration analyses, cells were plated for 2 h and then imaged using an HCX Plan Fluotar 10×/0.30 NA objective and a Nikon TE2000 microscope equipped with a humidified environmental chamber maintained at 37°C with 5% CO_2. Images were acquired at 10-min intervals in four or five fields per well. Inhibitor-treated cells were imaged for 4 h following addition of the inhibitor/DMSO. Cells that remained in frame and did not contact other cells throughout the duration of the movie were selected for analysis using the FIJI manual tracker plug-in to track cell movement and to calculate migration velocity and directionality of each cell.

Statistical analyses

Two-tailed unpaired Student's *t* tests were performed using Excel for comparison between two experimental groups for most experiments, except where stated otherwise. One-tailed unpaired Student's *t* tests were utilized to assess whether treatments with an expected direction of effect promoted either increased (formin inhibition) or decreased (Hic-5 overexpression, Cdc42 inhibition) migration velocity. For radial distribution of vimentin, the *p* value was calculated from a nested mixed-effects model. Both models include a fixed intercept, slope, and curvature (a parabolic fit) and an image-stratified random effect on the intercept and the slope. The nested model adds an interaction between experimental condition and curvature, allowing statistical comparison of shifts in the peak of the curve representing vimentin fluorescence radial distribution. Models were fitted using the lme4 library and *p* values were derived from the analysis of variance function in both the statistical programming language and environment R (Bates *et al.*, 2015). Data sets

were acquired from three or more independent experiments, except where otherwise indicated. *, $p < 0.05$; **, $p < 0.01$; ***, $p < 0.001$; and ****, $p < 0.0001$. Data are graphed as averages with error bars indicating SEM, except for MT dynamics data, which are graphed as a box-and-whisker plot where the bounds of the box represent the interquartile range, the horizontal line within the box represents the median, and the whiskers represent the range of the data.

ACKNOWLEDGMENTS

We thank past and present members of the Turner, Sexton, Speliotes, Bernstein, Ridilla, and Shea labs for helpful discussion of the data. We also thank Edward Boumil and Audrey Bernstein (SUNY Upstate Medical University) for tubulin antibodies and Jessica Henty-Ridilla (SUNY Upstate Medical University) for providing EMTD and EB1 plasmids. This work was supported by National Institutes of Health Grants RO1GM047607 and R35GM131709 to C.E.T.

REFERENCES

Abercrombie M, Heaysman JE, Pegrum SM (1970a). The locomotion of fibroblasts in culture: I. Movements of the leading edge. Exp Cell Res 59, 393–398.

Abercrombie M, Heaysman JE, Pegrum SM (1970b). The locomotion of fibroblasts in culture: II. "Ruffling." Exp Cell Res 60, 437–444.

Abercrombie M, Heaysman JE, Pegrum SM (1970c). The locomotion of fibroblasts in culture: III. Movements of particles on the dorsal surface of the leading lamella. Exp Cell Res 62, 389–398.

Albrengues J, Bertero T, Grasset E, Bonan S, Maiel M, Bourget I, Philippe C, Herraiz Serrano C, Benamar S, Croce O, *et al*. (2015). Epigenetic switch drives the conversion of fibroblasts into proinvasive cancer-associated fibroblasts. Nat Commun 6, 10204.

Anderson TW, Vaughan AN, Cramer LP (2008). Retrograde flow and myosin II activity within the leading cell edge deliver F-actin to the lamella to seed the formation of graded polarity actomyosin II filament bundles in migrating fibroblasts. Mol Biol Cell 19, 5006–5018.

Applegate KT, Besson S, Matov A, Bagonis MH, Jaqaman K, Danuser G (2011). plusTipTracker: quantitative image analysis software for the measurement of microtubule dynamics. J Struct Biol 176, 168–184.

Bates D, Mächler M, Bolker B, Walker S (2015). Fitting linear mixed-effects models using lme4. J Stat Softw 67, 1–48.

Bershadsky AD, Vaisberg EA, Vasiliev JM (1991). Pseudopodial activity at the active edge of migrating fibroblast is decreased after drug-induced microtubule depolymerization. Cell Motil Cytoskeleton 19, 152–158.

Bhattacharya R, Gonzalez AM, Debiase PJ, Trejo HE, Goldman RD, Flitney FW, Jones JC (2009). Recruitment of vimentin to the cell surface by beta3 integrin and plectin mediates adhesion strength. J Cell Sci 122, 1390–1400.

Blangy A (2017). Tensins are versatile regulators of Rho GTPase signalling and cell adhesion. Biol Cell 109, 115–126.

Breitsprecher D, Goode BL (2013). Formins at a glance. J Cell Sci 126, 1–7.

Brown MC, Turner CE (2004). Paxillin: adapting to change. Physiol Rev 84, 1315–1339.

Burgstaller G, Gregor M, Winter L, Wiche G (2010). Keeping the vimentin network under control: cell-matrix adhesion-associated plectin 1f affects cell shape and polarity of fibroblasts. Mol Biol Cell 21, 3362–3375.

Burridge K, Guilluy C (2016). Focal adhesions, stress fibers and mechanical tension. Exp Cell Res 343, 14–20.

Campbell JJ, Knight MM (2007). An improved confocal FRAP technique for the measurement of long-term actin dynamics in individual stress fibers. Microsc Res Tech 70, 1034–1040.

Carpenter AE, Jones TR, Lamprecht MR, Clarke C, Kang IH, Friman O, Guertin DA, Chang JH, Lindquist RA, Moffat J, *et al*. (2006). CellProfiler: image analysis software for identifying and quantifying cell phenotypes. Genome Biol 7, R100.

Castanon MJ, Walko G, Winter L, Wiche G (2013). Plectin–intermediate filament partnership in skin, skeletal muscle, and peripheral nerve. Histochem Cell Biol 140, 33–53.

Chan W, Kozma R, Yasui Y, Inagaki M, Leung T, Manser E, Lim L (2002). Vimentin intermediate filament reorganization by Cdc42: involvement of PAK and p70 S6 kinase. Eur J Cell Biol 81, 692–701.

Cheng TJ, Tseng YF, Chang WM, Chang MD, Lai YK (2003). Retaining of the assembly capability of vimentin phosphorylated by mitogen-activated protein kinase-activated protein kinase-2. J Cell Biochem 89, 589–602.

Chernoivanenko IS, Matveeva EA, Gelfand VI, Goldman RD, Minin AA (2015). Mitochondrial membrane potential is regulated by vimentin intermediate filaments. FASEB J 29, 820–827.

Colburn ZT, Jones JCR (2018). Complexes of alpha6beta4 integrin and vimentin act as signaling hubs to regulate epithelial cell migration. J Cell Sci 131.

Costigliola N, Ding L, Burckhardt CJ, Han SJ, Gutierrez E, Mota A, Groisman A, Mitchison TJ, Danuser G (2017). Vimentin fibers orient traction stress. Proc Natl Acad Sci USA 114, 5195–5200.

Dabiri G, Tumbarello DA, Turner CE, Van de Water L (2008). Hic-5 promotes the hypertrophic scar myofibroblast phenotype by regulating the TGF-beta1 autocrine loop. J Invest Dermatol 128, 2518–2525.

Deakin NO, Ballestrem C, Turner CE (2012). Paxillin and Hic-5 interaction with vinculin is differentially regulated by Rac1 and RhoA. PLoS One 7, e37990.

Deakin NO, Bass MD, Warwood S, Schoelermann J, Mostafavi-Pour Z, Knight D, Ballestrem C, Humphries MJ (2009). An integrin-alpha4-14-3-3zeta-paxillin ternary complex mediates localised Cdc42 activity and accelerates cell migration. J Cell Sci 122, 1654–1664.

Deakin NO, Turner CE (2008). Paxillin comes of age. J Cell Sci 121, 2435–2444.

Deakin NO, Turner CE (2011). Distinct roles for paxillin and Hic-5 in regulating breast cancer cell morphology, invasion, and metastasis. Mol Biol Cell 22, 327–341.

Deakin NO, Turner CE (2014). Paxillin inhibits HDAC6 to regulate microtubule acetylation, Golgi structure, and polarized migration. J Cell Biol 206, 395–413.

Eckes B, Colucci-Guyon E, Smola H, Nodder S, Babinet C, Krieg T, Martin P (2000). Impaired wound healing in embryonic and adult mice lacking vimentin. J Cell Sci 113 (Pt 13), 2455–2462.

Eckes B, Dogic D, Colucci-Guyon E, Wang N, Maniotis A, Ingber D, Merckling A, Langa F, Aumailley M, Delouvee A, *et al*. (1998). Impaired mechanical stability, migration and contractile capacity in vimentin-deficient fibroblasts. J Cell Sci 111 (Pt 13), 1897–1907.

Efimov A, Schiefermeier N, Grigoriev I, Ohi R, Brown MC, Turner CE, Small JV, Kaverina I (2008). Paxillin-dependent stimulation of microtubule catastrophes at focal adhesion sites. J Cell Sci 121, 196–204.

Engel A, Eichner R, Aebi U (1985). Polymorphism of reconstituted human epidermal keratin filaments: determination of their mass-per-length and width by scanning transmission electron microscopy (STEM). J Ultrastruct Res 90, 323–335.

Eriksson JE, Dechat T, Grin B, Helfand B, Mendez M, Pallari HM, Goldman RD (2009). Introducing intermediate filaments: from discovery to disease. J Clin Invest 119, 1763–1771.

Eriksson JE, He T, Trejo-Skalli AV, Harmala-Brasken AS, Hellman J, Chou YH, Goldman RD (2004). Specific in vivo phosphorylation sites determine the assembly dynamics of vimentin intermediate filaments. J Cell Sci 117, 919–932.

Ezratty EJ, Partridge MA, Gundersen GG (2005). Microtubule-induced focal adhesion disassembly is mediated by dynamin and focal adhesion kinase. Nat Cell Biol 7, 581–590.

Friedl P, Wolf K (2003). Tumour-cell invasion and migration: diversity and escape mechanisms. Nat Rev Cancer 3, 362–374.

Friedl P, Wolf K (2010). Plasticity of cell migration: a multiscale tuning model. J Cell Biol 188, 11–19.

Friesland A, Zhao Y, Chen YH, Wang L, Zhou H, Lu Q (2013). Small molecule targeting Cdc42-intersectin interaction disrupts Golgi organization and suppresses cell motility. Proc Natl Acad Sci USA 110, 1261–1266.

Gan Z, Ding L, Burckhardt CJ, Lowery J, Zaritsky A, Sitterley K, Mota A, Costigliola N, Starker CG, Voytas DF, *et al*. (2016). Vimentin intermediate filaments template microtubule networks to enhance persistence in cell polarity and directed migration. Cell Syst 3, 500–501.

Gardel ML, Sabass B, Ji L, Danuser G, Schwarz US, Waterman CM (2008). Traction stress in focal adhesions correlates biphasically with actin retrograde flow speed. J Cell Biol 183, 999–1005.

Gardel ML, Schneider IC, Aratyn-Schaus Y, Waterman CM (2010). Mechanical integration of actin and adhesion dynamics in cell migration. Annu Rev Cell Dev Biol 26, 315–333.

Goldman RD (1971). The role of three cytoplasmic fibers in BHK-21 cell motility. I. Microtubules and the effects of colchicine. J Cell Biol 51, 752–762.

Goreczny GJ, Forsythe IJ, Turner CE (2018). Hic-5 regulates fibrillar adhesion formation to control tumor extracellular matrix remodeling through interaction with tensin1. Oncogene 37, 1699–1713.
Goreczny GJ, Ouderkirk-Pecone JL, Olson EC, Krendel M, Turner CE (2017). Hic-5 remodeling of the stromal matrix promotes breast tumor progression. Oncogene 36, 2693–2703.
Goto H, Kosako H, Tanabe K, Yanagida M, Sakurai M, Amano M, Kaibuchi K, Inagaki M (1998). Phosphorylation of vimentin by Rho-associated kinase at a unique amino-terminal site that is specifically phosphorylated during cytokinesis. J Biol Chem 273, 11728–11736.
Goto H, Tanabe K, Manser E, Lim L, Yasui Y, Inagaki M (2002). Phosphorylation and reorganization of vimentin by p21-activated kinase (PAK). Genes Cells 7, 91–97.
Goto H, Yasui Y, Kawajiri A, Nigg EA, Terada Y, Tatsuka M, Nagata K, Inagaki M (2003). Aurora-B regulates the cleavage furrow-specific vimentin phosphorylation in the cytokinetic process. J Biol Chem 278, 8526–8530.
Gregor M, Osmanagic-Myers S, Burgstaller G, Wolfram M, Fischer I, Walko G, Resch GP, Jorgl A, Herrmann H, Wiche G (2014). Mechanosensing through focal adhesion-anchored intermediate filaments. FASEB J 28, 715–729.
Gulvady AC, Dubois F, Deakin NO, Goreczny GJ, Turner CE (2018). Hic-5 expression is a major indicator of cancer cell morphology, migration, and plasticity in three-dimensional matrices. Mol Biol Cell 29, 1704–1717.
Guo M, Ehrlicher AJ, Jensen MH, Renz M, Moore JR, Goldman RD, Lippincott-Schwartz J, Mackintosh FC, Weitz DA (2014). Probing the stochastic, motor-driven properties of the cytoplasm using force spectrum microscopy. Cell 158, 822–832.
Haage A, Goodwin K, Whitewood A, Camp D, Bogutz A, Turner CT, Granville DJ, Lefebvre L, Plotnikov S, Goult BT, Tanentzapf G (2018). Talin autoinhibition regulates cell–ECM adhesion dynamics and wound healing in vivo. Cell Rep 25, 2401–2416.e2405.
Hagel M, George EL, Kim A, Tamimi R, Opitz SL, Turner CE, Imamoto A, Thomas SM (2002). The adaptor protein paxillin is essential for normal development in the mouse and is a critical transducer of fibronectin signaling. Mol Cell Biol 22, 901–915.
Havel LS, Kline ER, Salgueiro AM, Marcus AI (2015). Vimentin regulates lung cancer cell adhesion through a VAV2-Rac1 pathway to control focal adhesion kinase activity. Oncogene 34, 1979–1990.
Heitzer MD, DeFranco DB (2006). Hic-5/ARA55, a LIM domain-containing nuclear receptor coactivator expressed in prostate stromal cells. Cancer Res 66, 7326–7333.
Helfand BT, Mendez MG, Murthy SN, Shumaker DK, Grin B, Mahammad S, Aebi U, Wedig T, Wu YI, Hahn KM, *et al*. (2011). Vimentin organization modulates the formation of lamellipodia. Mol Biol Cell 22, 1274–1289.
Helfand BT, Mendez MG, Pugh J, Delsert C, Goldman RD (2003). A role for intermediate filaments in determining and maintaining the shape of nerve cells. Mol Biol Cell 14, 5069–5081.
Hollenbeck PJ, Bershadsky AD, Pletjushkina OY, Tint IS, Vasiliev JM (1989). Intermediate filament collapse is an ATP-dependent and actin-dependent process. J Cell Sci 92 (Pt 4), 621–631.
Hotulainen P, Lappalainen P (2006). Stress fibers are generated by two distinct actin assembly mechanisms in motile cells. J Cell Biol 173, 383–394.
Huber F, Boire A, Lopez MP, Koenderink GH (2015). Cytoskeletal crosstalk: when three different personalities team up. Curr Opin Cell Biol 32, 39–47.
Inagaki N, Katsuno H (2017). Actin waves: origin of cell polarization and migration? Trends Cell Biol 27, 515–526.
Janosch P, Kieser A, Eulitz M, Lovric J, Sauer G, Reichert M, Gounari F, Buscher D, Baccarini M, Mischak H, Kolch W (2000). The Raf-1 kinase associates with vimentin kinases and regulates the structure of vimentin filaments. FASEB J 14, 2008–2021.
Jaqaman K, Loerke D, Mettlen M, Kuwata H, Grinstein S, Schmid SL, Danuser G (2008). Robust single-particle tracking in live-cell time-lapse sequences. Nat Methods 5, 695–702.
Jeganathan N, Predescu D, Zhang J, Sha F, Bardita C, Patel M, Wood S, Borgia JA, Balk RA, Predescu S (2016). Rac1-mediated cytoskeleton rearrangements induced by intersectin-1s deficiency promotes lung cancer cell proliferation, migration and metastasis. Mol Cancer 15, 59.
Jiu Y, Lehtimaki J, Tojkander S, Cheng F, Jaalinoja H, Liu X, Varjosalo M, Eriksson JE, Lappalainen P (2015). Bidirectional interplay between vimentin intermediate filaments and contractile actin stress fibers. Cell Rep 11, 1511–1518.
Jones TR, Kang IH, Wheeler DB, Lindquist RA, Papallo A, Sabatini DM, Golland P, Carpenter AE (2008). CellProfiler Analyst: data exploration and analysis software for complex image-based screens. BMC Bioinformatics 9, 482.
Kage F, Winterhoff M, Dimchev V, Mueller J, Thalheim T, Freise A, Bruhmann S, Kollasser J, Block J, Dimchev G, *et al*. (2017). FMNL formins boost lamellipodial force generation. Nat Commun 8, 14832.
Kakade PS, Budnar S, Kalraiya RD, Vaidya MM (2016). Functional implications of O-GlcNAcylation-dependent phosphorylation at a proximal site on keratin 18. J Biol Chem 291, 12003–12013.
Kalluri R (2016). The biology and function of fibroblasts in cancer. Nat Rev Cancer 16, 582–598.
Katsuno H, Toriyama M, Hosokawa Y, Mizuno K, Ikeda K, Sakumura Y, Inagaki N (2015). Actin migration driven by directional assembly and disassembly of membrane-anchored actin filaments. Cell Rep 12, 648–660.
Kaverina I, Rottner K, Small JV (1998). Targeting, capture, and stabilization of microtubules at early focal adhesions. J Cell Biol 142, 181–190.
Kholmanskikh SS, Dobrin JS, Wynshaw-Boris A, Letourneau PC, Ross ME (2003). Disregulated RhoGTPases and actin cytoskeleton contribute to the migration defect in Lis1-deficient neurons. J Neurosci 23, 8673–8681.
Kidd ME, Shumaker DK, Ridge KM (2014). The role of vimentin intermediate filaments in the progression of lung cancer. Am J Respir Cell Mol Biol 50, 1–6.
Kim J, Yang C, Kim EJ, Jang J, Kim SJ, Kang SM, Kim MG, Jung H, Park D, Kim C (2016). Vimentin filaments regulate integrin-ligand interactions by binding to the cytoplasmic tail of integrin beta3. J Cell Sci 129, 2030–2042.
Kreis S, Schonfeld HJ, Melchior C, Steiner B, Kieffer N (2005). The intermediate filament protein vimentin binds specifically to a recombinant integrin alpha2/beta1 cytoplasmic tail complex and co-localizes with native alpha2/beta1 in endothelial cell focal adhesions. Exp Cell Res 305, 110–121.
Kuhn S, Geyer M (2014). Formins as effector proteins of Rho GTPases. Small GTPases 5, e29513.
Lammers M, Rose R, Scrima A, Wittinghofer A (2005). The regulation of mDia1 by autoinhibition and its release by Rho*GTP. EMBO J 24, 4176–4187.
Lauffenburger DA, Horwitz AF (1996). Cell migration: a physically integrated molecular process. Cell 84, 359–369.
LeBleu VS, Kalluri R (2018). A peek into cancer-associated fibroblasts: origins, functions and translational impact. Dis Model Mech 11, 1–9.
Leduc C, Etienne-Manneville S (2017). Regulation of microtubule-associated motors drives intermediate filament network polarization. J Cell Biol 216, 1689–1703.
Leube RE, Moch M, Windoffer R (2015). Intermediate filaments and the regulation of focal adhesion. Curr Opin Cell Biol 32, 13–20.
Li L, He Y, Zhao M, Jiang J (2013). Collective cell migration: implications for wound healing and cancer invasion. Burns Trauma 1, 21–26.
Li QF, Spinelli AM, Wang R, Anfinogenova Y, Singer HA, Tang DD (2006). Critical role of vimentin phosphorylation at Ser-56 by p21-activated kinase in vimentin cytoskeleton signaling. J Biol Chem 281, 34716–34724.
Liu BP, Burridge K (2000). Vav2 activates Rac1, Cdc42, and RhoA downstream from growth factor receptors but not beta1 integrins. Mol Cell Biol 20, 7160–7169.
Liu CY, Lin HH, Tang MJ, Wang YK (2015). Vimentin contributes to epithelial-mesenchymal transition cancer cell mechanics by mediating cytoskeletal organization and focal adhesion maturation. Oncotarget 6, 15966–15983.
Livne A, Geiger B (2016). The inner workings of stress fibers—from contractile machinery to focal adhesions and back. J Cell Sci 129, 1293–1304.
Lloyd CW, Smith CG, Woods A, Rees DA (1977). Mechanisms of cellular adhesion. II. The interplay between adhesion, the cytoskeleton and morphology in substrate-attached cells. Exp Cell Res 110, 427–437.
Lowery J, Kuczmarski ER, Herrmann H, Goldman RD (2015). Intermediate filaments play a pivotal role in regulating cell architecture and function. J Biol Chem 290, 17145–17153.
Madsen CD, Sahai E (2010). Cancer dissemination—lessons from leukocytes. Dev Cell 19, 13–26.
Matsukawa T, Morita K, Omizu S, Kato S, Koriyama Y (2018). Mechanisms of RhoA inactivation and CDC42 and Rac1 activation during zebrafish optic nerve regeneration. Neurochem Int 112, 71–80.

Menko AS, Bleaken BM, Libowitz AA, Zhang L, Stepp MA, Walker JL (2014). A central role for vimentin in regulating repair function during healing of the lens epithelium. Mol Biol Cell 25, 776–790.
Meriane M, Mary S, Comunale F, Vignal E, Fort P, Gauthier-Rouviere C (2000). Cdc42Hs and Rac1 GTPases induce the collapse of the vimentin intermediate filament network. J Biol Chem 275, 33046–33052.
Miller AL, Bement WM (2009). Regulation of cytokinesis by Rho GTPase flux. Nat Cell Biol 11, 71–77.
Murray ME, Mendez MG, Janmey PA (2014). Substrate stiffness regulates solubility of cellular vimentin. Mol Biol Cell 25, 87–94.
Ng MR, Besser A, Danuser G, Brugge JS (2012). Substrate stiffness regulates cadherin-dependent collective migration through myosin-II contractility. J Cell Biol 199, 545–563.
Oakes PW, Wagner E, Brand CA, Probst D, Linke M, Schwarz US, Glotzer M, Gardel ML (2017). Optogenetic control of RhoA reveals zyxin-mediated elasticity of stress fibres. Nat Commun 8, 15817.
Omelyanchuk LV, Munzarova AF (2017). Theoretical model of mitotic spindle microtubule growth for FRAP curve interpretation. BMC Syst Biol 11, 378.
Osmanagic-Myers S, Rus S, Wolfram M, Brunner D, Goldmann WH, Bonakdar N, Fischer I, Reipert S, Zuzuarregui A, Walko G, Wiche G (2015). Plectin reinforces vascular integrity by mediating crosstalk between the vimentin and the actin networks. J Cell Sci 128, 4138–4150.
Pankov R, Cukierman E, Katz BZ, Matsumoto K, Lin DC, Lin S, Hahn C, Yamada KM (2000). Integrin dynamics and matrix assembly: tensin-dependent translocation of alpha(5)beta(1) integrins promotes early fibronectin fibrillogenesis. J Cell Biol 148, 1075–1090.
Patteson AE, Pogoda K, Byfield FJ, Charrier EE, Galie PA, Deptuła P, Bucki R, Janmey PA (2018). Loss of vimentin intermediate filaments decreases peri-nuclear stiffness and enhances cell motility through confined spaces, arXiv:1807.06378 [physics.bio-ph].
Pignatelli J, Tumbarello DA, Schmidt RP, Turner CE (2012). Hic-5 promotes invadopodia formation and invasion during TGF-beta-induced epithelial-mesenchymal transition. J Cell Biol 197, 421–437.
Prahlad V, Yoon M, Moir RD, Vale RD, Goldman RD (1998). Rapid movements of vimentin on microtubule tracks: kinesin-dependent assembly of intermediate filament networks. J Cell Biol 143, 159–170.
Rane CK, Minden A (2014). P21 activated kinases: structure, regulation, and functions. Small GTPases 5, e28003.
Rasanen K, Vaheri A (2010). Activation of fibroblasts in cancer stroma. Exp Cell Res 316, 2713–2722.
Rathje LS, Nordgren N, Pettersson T, Ronnlund D, Widengren J, Aspenstrom P, Gad AK (2014). Oncogenes induce a vimentin filament collapse mediated by HDAC6 that is linked to cell stiffness. Proc Natl Acad Sci USA 111, 1515–1520.
Ridley AJ (2015). Rho GTPase signalling in cell migration. Curr Opin Cell Biol 36, 103–112.
Ridley AJ, Schwartz MA, Burridge K, Firtel RA, Ginsberg MH, Borisy G, Parsons JT, Horwitz AR (2003). Cell migration: integrating signals from front to back. Science 302, 1704–1709.
Rizvi SA, Neidt EM, Cui J, Feiger Z, Skau CT, Gardel ML, Kozmin SA, Kovar DR (2009). Identification and characterization of a small molecule inhibitor of formin-mediated actin assembly. Chem Biol 16, 1158–1168.
Rose R, Weyand M, Lammers M, Ishizaki T, Ahmadian MR, Wittinghofer A (2005). Structural and mechanistic insights into the interaction between Rho and mammalian Dia. Nature 435, 513–518.
Sawant M, Schwarz N, Windoffer R, Magin TM, Krieger J, Mucke N, Obara B, Jankowski V, Jankowski J, Wally V, *et al*. (2018). Threonine 150 Phosphorylation of keratin 5 is linked to epidermolysis bullosa simplex and regulates filament assembly and cell viability. J Invest Dermatol 138, 627–636.
Saxton WM, Stemple DL, Leslie RJ, Salmon ED, Zavortink M, McIntosh JR (1984). Tubulin dynamics in cultured mammalian cells. J Cell Biol 99, 2175–2186.
Scarpa E, Mayor R (2016). Collective cell migration in development. J Cell Biol 212, 143–155.
Seluanov A, Vaidya A, Gorbunova V (2010). Establishing primary adult fibroblast cultures from rodents. J Vis Exp 44, e2033.
Shea TB (1990). Transient increase in vimentin in axonal cytoskeletons during differentiation in NB2a/d1 cells. Brain Res 521, 338–342.
Shibanuma M, Mashimo J, Kuroki T, Nose K (1994). Characterization of the TGF beta 1-inducible hic-5 gene that encodes a putative novel zinc finger protein and its possible involvement in cellular senescence. J Biol Chem 269, 26767–26774.
Shiga K, Hara M, Nagasaki T, Sato T, Takahashi H, Takeyama H (2015). Cancer-associated fibroblasts: their characteristics and their roles in tumor growth. Cancers (Basel) 7, 2443–2458.
Sixt M (2012). Cell migration: fibroblasts find a new way to get ahead. J Cell Biol 197, 347–349.
Small JV, Stradal T, Vignal E, Rottner K (2002). The lamellipodium: where motility begins. Trends Cell Biol 12, 112–120.
Snider NT, Omary MB (2014). Post-translational modifications of intermediate filament proteins: mechanisms and functions. Nat Rev Mol Cell Biol 15, 163–177.
Spiering D, Hodgson L (2011). Dynamics of the Rho-family small GTPases in actin regulation and motility. Cell Adh Migr 5, 170–180.
Terriac E, Coceano G, Mavajian Z, Hageman TA, Christ AF, Testa I, Lautenschlager F, Gad AK (2017). Vimentin levels and serine 71 phosphorylation in the control of cell–matrix adhesions, migration speed, and shape of transformed human fibroblasts. Cells 6, 1–13.
Tsui C, Maldonado P, Montaner B, Borroto A, Alarcon B, Bruckbauer A, Martinez-Martin N, Batista FD (2018). Dynamic reorganisation of intermediate filaments coordinates early B-cell activation. Life Sci Alliance 1, e201800060.
Tsujimura K, Ogawara M, Takeuchi Y, Imajoh-Ohmi S, Ha MH, Inagaki M (1994). Visualization and function of vimentin phosphorylation by cdc2 kinase during mitosis. J Biol Chem 269, 31097–31106.
Tsuruta D, Jones JC (2003). The vimentin cytoskeleton regulates focal contact size and adhesion of endothelial cells subjected to shear stress. J Cell Sci 116, 4977–4984.
Tumbarello DA, Turner CE (2007). Hic-5 contributes to epithelial-mesenchymal transformation through a RhoA/ROCK-dependent pathway. J Cell Physiol 211, 736–747.
Turner CE (2000). Paxillin and focal adhesion signalling. Nat Cell Biol 2, E231–E236.
Vallenius T (2013). Actin stress fibre subtypes in mesenchymal-migrating cells. Open Biol 3, 130001.
Vohnoutka RB, Boumil EF, Liu Y, Uchida A, Pant HC, Shea TB (2017). Influence of a GSK3beta phosphorylation site within the proximal C-terminus of neurofilament-H on neurofilament dynamics. Biol Open 6, 1516–1527.
Vuoriluoto K, Haugen H, Kiviluoto S, Mpindi JP, Nevo J, Gjerdrum C, Tiron C, Lorens JB, Ivaska J (2011). Vimentin regulates EMT induction by Slug and oncogenic H-Ras and migration by governing Axl expression in breast cancer. Oncogene 30, 1436–1448.
Wang H, Song K, Krebs TL, Yang J, Danielpour D (2008). Smad7 is inactivated through a direct physical interaction with the LIM protein Hic-5/ARA55. Oncogene 27, 6791–6805.
Weed SA, Karginov AV, Schafer DA, Weaver AM, Kinley AW, Cooper JA, Parsons JT (2000). Cortactin localization to sites of actin assembly in lamellipodia requires interactions with F-actin and the Arp2/3 complex. J Cell Biol 151, 29–40.
Wei J, Xu G, Wu M, Zhang Y, Li Q, Liu P, Zhu T, Song A, Zhao L, Han Z *et al*. (2008). Overexpression of vimentin contributes to prostate cancer invasion and metastasis via src regulation. Anticancer Res 28, 327–334.
Yamaguchi T, Goto H, Yokoyama T, Sillje H, Hanisch A, Uldschmid A, Takai Y, Oguri T, Nigg EA, Inagaki M (2005). Phosphorylation by Cdk1 induces Plk1-mediated vimentin phosphorylation during mitosis. J Cell Biol 171, 431–436.
Yasui Y, Goto H, Matsui S, Manser E, Lim L, Nagata K, Inagaki M (2001). Protein kinases required for segregation of vimentin filaments in mitotic process. Oncogene 20, 2868–2876.
Yoon M, Moir RD, Prahlad V, Goldman RD (1998). Motile properties of vimentin intermediate filament networks in living cells. J Cell Biol 143, 147–157.
Yu JA, Deakin NO, Turner CE (2010). Emerging role of paxillin-PKL in regulation of cell adhesion, polarity and migration. Cell Adh Migr 4, 342–347.
Yue J, Xie M, Gou X, Lee P, Schneider MD, Wu X (2014). Microtubules regulate focal adhesion dynamics through MAP4K4. Dev Cell 31, 572–585.
Zamir E, Katz M, Posen Y, Erez N, Yamada KM, Katz BZ, Lin S, Lin DC, Bershadsky A, Kam Z, Geiger B (2000). Dynamics and segregation of cell-matrix adhesions in cultured fibroblasts. Nat Cell Biol 2, 191–196.
Zhang Y, Zhang H, Yuan X, Gu X (2007). Differential effects of phenylalanine on Rac1, Cdc42, and RhoA expression and activity in cultured cortical neurons. Pediatr Res 62, 8–13.
Zhu QS, Rosenblatt K, Huang KL, Lahat G, Brobey R, Bolshakov S, Nguyen T, Ding Z, Belousov R, Bill K, *et al*. (2011). Vimentin is a novel AKT1 target mediating motility and invasion. Oncogene 30, 457–470.